

# Surface alignment control of nematodynamics

C. J. Holmes<sup>1</sup>

<sup>1</sup>School of Physics, University of Exeter, Stocker Road, Exeter, EX4 4QL, UK\*

The primary study of this thesis is the response of the nematic director to pressure driven flow. Dynamic flow experiments using optical conoscopy and pressure gradient measurements are used to explore the physics behind the flow alignment seen to occur for some nematic liquid crystals. New research into the techniques and methods for aligning the director at a glass interface is also presented, the results of which are used towards the latter end of this thesis in the production of a highly novel flow cell. A bespoke technique for fabricating robust liquid crystal flow cells is also presented.

The observation of flow alignment for the nematic liquid crystal 5CB is detailed for pressure driven flow via optical conoscopy when the director is initially aligned planar homogeneously at 45° to the direction of flow. The results of this experiment are compared to the theory of Ericksen and Leslie through a one dimensional dynamic model that provides simulated director profiles and corresponding simulated conoscopic images. Good agreement between the data and simulation is observed, whereby the director is seen to rotate to become parallel to the flow direction whilst exhibiting no net tilt distortion at all flow rates.

The presence of small surface pretilt from a rubbed planar aligning polyimide layer and its effect on director rotation is also examined for cells that are rubbed in both the parallel and anti-parallel directions. The result observed is a striking difference in the mean director rotation when initially aligned close to normal to the direction of flow. The results of these experiments are also compared to the theory of Ericksen and Leslie through the one dimensional dynamic model. Good agreement is seen, highlighting the dramatic effect that a small amount of surface pretilt can have on the overall director orientation, whilst also demonstrating the need for caution when assuming that rubbed conventional alignment techniques provide true planar orientation.

Two methods for producing intermediate or large pretilt angles at liquid crystal alignment surfaces are also examined. Here, two recipes involving the commercial polyimides Nissan SE-1211, Nissan SE-130 and Nissan SE-4811 are experimentally investigated, with results showing the ability to tune the director pretilt angle as a function of the rubbing strength used to align the sample. The results also show an interesting dependance on the material upon which the aligning layer is deposited for the recipe involving Nissan SE-1211. Here, vastly different pretilt angles are observed for cells constructed with glass and indium tin oxide (ITO) layers.

Finally, the large pretilt angles produced from the recipes mentioned above are also used to fabricate pressure driven flow cells exhibiting large pretilt angles on both surfaces, constraining the director to align in a splayed state. When aligned parallel to the flow direction, experiments examining the valve-like nature of the director profile suggest that a preferential flow direction exists in what here is termed the ‘diode cell’. Measurements of the pressure gradient required to achieve a constant volumetric flow rate through the cell are compared for flow in both directions relative to the splayed director profile. A striking difference is observed for flow ‘with’ the splay and ‘against’ the splay, leading to the realisation of a cell exhibiting a preferential flow direction through surface treatment. Again, results are compared to the theory of Ericksen and Leslie through the one dimensional dynamic model, showing good agreement.

## CONTENTS

I. Acknowledgements	ii	IV. Theory / Methods	7
II. Introduction	1	A. Introduction	7
A. Thesis outline	1	B. Background	7
III. The Liquid Crystalline phase of matter	3	C. Constitutive equations and the Leslie viscosities	7
A. Thermotropic liquid crystals	3	D. Comments and Constraints on the Leslie viscosities	8
B. Nematic liquid crystals	3	E. The Parodi relation	9
C. Nematic Order	4	F. Flow-alignment (“logs in rivers”)	9
D. Optical Anisotropy	4	G. Simplified flow-alignment	10
E. Dielectric Anisotropy	5	H. A 1-D numerical model of liquid crystal dynamics	12
F. Elastic Constants and Free Energy	5	1. Assumptions	12
G. Surface alignment	5	I. The Leslie-Ericksen equations	12
		J. Twist	12
		K. Tilt	13

L. Flow field	13
M. Conoscopy	14
N. Simulation	14
O. Experimental	15
P. Planar alignment - rotating the cell	16
Q. Planar alignment - rotating the polarisers	16
R. Planar alignment - thickness variation	17
S. Vertical alignment	18
T. Polarisers crossed and parallel	18
U. Tracking conoscopic figure alignment	18
V. Cell fabrication	19
W. Microscope slide preparation	19
X. Cell construction	20
References	23
V. Alex	24

## I. ACKNOWLEDGEMENTS

I would like to take this opportunity to say a genuine and heart-felt thank you to the many people who helped me on the way to finally completing this thesis.

Firstly, of course, I thank my supervisor Professor Roy Sambles. The road to this thesis hasn't always been easy, but Roy has helped me put things into perspective on more than one occasion, and for that I am truly grateful. It has not only been your ability to instantly spot the solution to my problems, but also your ability to instantly spot when I've been surfing rather than in the lab, that has kept me on my toes throughout the last three years. Thank you.

Secondly, I must say a special thank you to Stephen Cornford. If it were not for both your immense understanding of liquid crystal dynamics and your immense ability to explain complex problems to me in a way in which I can understand, this Ph.D would not have been possible. Your razor sharp wit has also not gone unnoticed. I must also apologise for the barrage of messages you received once I'd started writing up this thesis, when I was having a panic attack almost daily. Thank you Steph.

I must also say a special thank you to the displays team at Hewlett Packard Labs in Bristol. I gratefully acknowledge the genuine interest and help that I received at our CASE meetings. I can honestly say that I felt welcome and part of the team almost instantly. A special mention must go to Tim Taphouse for being an all round source of technical expertise as well as being a fantastic mentor, and also to Steve Kitson for always taking the time to help out and always providing the solution to the problem at hand. Fantastic input was almost always provided by everyone in the group with particular reference to Adrian Geisow and Chris Newton. Of course, the ECLC 2011 in Slovenia would not have been as enjoyable without the 'mothering' provided by Suzanna Klein

and the perpetual moaning provided by Rob 'hang-time' Greasty. Thank you.

A big thank you must also go to Benny Hallam for being very understanding in giving me time to finish writing when I started work in Cornwall.

Next, as is customary, I would like to thank the more senior members of the Electromagnetic Materials Group at Exeter. Firstly, what can I say? Matthew (Lockers, Lockertron, Stocker, LockHeart) Lockyear RCE. Perhaps the less said here the better. Just remember this, '*what's said in the water, stays in the water*'. Next I must say thank you to Alistair 'Hello there' Hibbins for all the comic moments and home-brew help. I can't wait to see what you cook up for the next Great Physics Beer Festival. Thank you to Ian 'Hoop-dream' Hooper NRC. For you I have just one question, just one, it's a question that everyone is dying to know the answer too, something that I haven't been brave enough to ask you over the last three years ..... vodka ball? A special thank you also to both Fuzi and Lizhen, whether we were discussing my previous girlfriends, or a bowl of 2000 year old soup from an ancient chinese grave, I was always having fun. Sharon Jewell for all the help and advice at the start of my 'three years', it's fair to say that you taught me almost everything I know about making liquid crystal cells, and you were right, about 1 in 4 did work! Tim Atherton for your 'long range' helpful conversations, listening ear and computational expertise! Euan Hendry for regularly taking all my money in late night poker sessions. Pete V for the sound life advice and that one good surf at Putsborough, hopefully we'll get in again sometime. Bill Barnes for not only being an all round source of help, but for being my first tutor as an undergraduate physicist and firmly setting me on the path to continuing in Physics. Andy Murray for tea time chat and that one good surf at Dawlish Warren, keep it up (the sea will get warmer in the summer)! Tomeck for all the figure conversion that you made possible. Much appreciated! Evgeny Sirokin for being a fantastic Russian role model. I've never known anyone with a stronger hand shake or a firmer hug and pat on the back. Tom Isaac for being a source of much humour and good will, and to Nick Cole, without you I wouldn't have any samples or any shiny metal things to play with. We started at near enough the same day, and I have to say it's gone very fast, but thank you for all the technical expertise and advice. I must also say a big thank you to Alan Usher for agreeing to be my mentor at such short notice, and after just one meeting, helping me feel much better about my Ph. D.

Throughout my undergraduate time at Exeter, I made some great friends in Physics that also went on to complete their Ph. Ds here at Exeter. These are Lemmy Steve, Chris 'Buzz' Burrows and James Edmunds. So I must say a big thank you to you guys for helping me through my time here as a Ph. D student. In particular Lemmy Steve for all the good years as MPhys lab partners and hopefully many more good years to come!

Next I come to a special section of my acknowledgements

ments. Team Basement. When I first started my Ph. D, a select few were chosen to dwell in the basement of the Physics department. Without natural light, cleanliness, or a chance of escape, we forged a special bond that many basement dwellers before us have also shared. So I must say a massive thank you to the original Team Basement for helping to keep me sane and providing me with some of the best memories of my time at Exeter. James Parsons, Caroline '*Simon, side step to your left*' Pouya (aka Jupiter) and Edmund Stone. Ed, I must say a special thank you for not actually killing me, and for all the help with R during the early days. You were a fantastic human drum kit and I hope our friendship continues long after our time at Exeter! Caroline I must also say thank you for expanding my musical horizons and making me a better all round individual. Maybe someday you'll like Radiohead?

Along with Team Basement, there were many new Ph. D starters in 2008. Over the last three years I feel I've made good friendships with all of you and would like to say a big thank you to Matt 'Biggatronic' Bigginton, you adonis! Mel Taylor, for helping me calm down when I started to panic about this thesis. Celia Butler for being an all round source of information and help, I'd love to go gliding some day. Last but not least, a special mention must go to Helen Rance RC for eating all my chocolate bourbons and teaching me how to cook, a bit.

Also, during my three years as a post graduate student, I have met many new starters. Unfortunately we haven't been able to spend a long time together, but I would like to say thank you to Dmitry Polyushkin, Lizzy Brock, Simon Berry, Chinna Devarapu (you have the best laugh in the world!), Al Murray, Matt Nixon, Tim Starkey RC and Joe Blackman, who made me realise that not everything is lost!

Who am I missing? I'm sure I'm missing someone important...oh yes! That's right, Alfred John Lethbridge. Well, what can I say? It seems strange to acknowledge you, since we are in fact the same person, but, '*sometimes....not always....but sometimes*'. Seriously, thanks for the sound advice and brilliant memories over the last two years. See you in China.

Penultimately I would like to thank The Stormers with which I had the insurmountable pleasure of living (and working) with for 2 years. Namely, Dr. Ciaran 'Stew-storm' Stewart RC, Thomas 'Constorm' Constant RC and Peter 'Halestorm' Hale. Ciaran, you are a fantastic chef and a fantastic person. Thank you for all the bacon sandwiches and cups of tea. Not only that, but for all the surfing memories and BBQs at Radstations. I will, forever, remember the day of ball-ache. Tom, you are in some ways, the epitomy of what a Stormer should be. A gentleman and a scholar. Thanks for the t-shirt which i'll never wear again, and maybe someday you'll be the subject of an award winning National Geographic photo. Finally Pete, i'm writing this with my chodorouy trousers on. Perhaps we should make the angle again? Definitely DON'T come in (thanks for the tea).

Finally I'd like to say a huge thank you to my Mum, Dad and Brother. If it wasn't for the science open day at Ridgeway school all those years ago, I may never have experienced the joy of watching a ping pong ball being levitated by a jet of air from a vacuum cleaner in reverse. That means I may have never developed an interest in Physics! But seriously, thank you for the constant love, support, help and advice.

## II INTRODUCTION

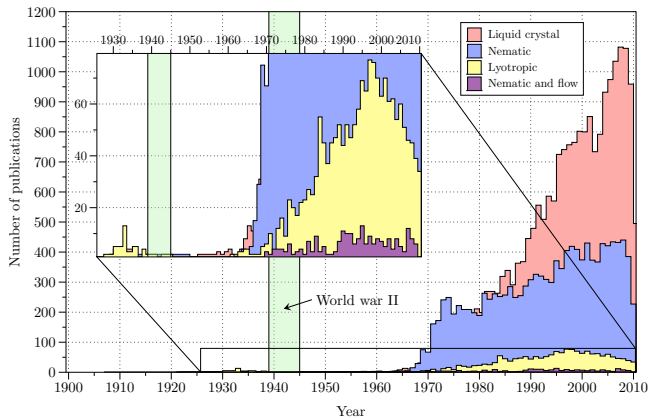


FIG. 1. A series of bar charts indicating the number of records on the Web of Science database that include in the article title the keyword shown in the legend. The lack of publications following World War II may be an artefact of the Web of Science database catalogue for these years. In any case, this figure serves to show the clear explosion in liquid crystal publication rates from 1970 onwards.

## II. INTRODUCTION

When Austrian born botanist Friedrich Reinitzer made the extraordinary observation in 1888 that a substance closely related to cholesterol had two melting points, one assumes he had no idea of the truly profound, awe-inspiring and beautiful branch of physics he was about to fore-father. His observation of a sample's transition from a solid crystal to a cloudy liquid at 145.5 °C and from a cloudy liquid to a clear liquid at 178.5 °C was without doubt, the first documented observation of the liquid crystalline phase of matter<sup>1,2</sup>.

In today's world, it's almost hard to believe that shortly after the second world war, scientific research in the field of liquid crystals slowed significantly due to the lack of a clear technological application. Conversely, at the time of writing, the majority of small to medium sized displays used worldwide are liquid crystal devices. With more liquid crystal displays (LCDs) (be it pocket calculator or flat screen television) in existence than there are people living on planet earth<sup>3</sup>, it is of no surprise that the LCD industry was worth more than 60 billion US dollars in 2006, with projections estimating three fold increases in the coming years<sup>3</sup>. With the explosion of interest and research carried out in the field of liquid crystals from the 1970s to present (see Figure 1), liquid crystal displays are now not only desired for their low cost, low power consumption and portability, but their attractiveness, ease of viewing and durability<sup>4</sup>.

However, as is the case with any 'state of the art' technology, it is destined to be quickly superseded by mankind's desire for faster, smaller, more efficient and simply better devices. With the new dawn in display screen technology arriving (OLEDs<sup>5</sup>) we still find use

for liquid crystal phases in other areas of science, as was highlighted recently at both the International Liquid Crystal Conference (ILCC 2010) in Kraków and the European Conference on Liquid Crystals (ECLC 2011) in Slovenia.

Recent work such as that of Fleury *et al.*<sup>6</sup> (the first winner of the Luckhurst Samulski prize<sup>7</sup>) is an excellent example of just how diverse and varied liquid crystal research can be. In their research, defect lines in nematic liquid crystal textures have been used to build metallic microwires, which allow for highly accurate electrode connections to be fabricated, down to the order of a few micrometers. This however, is just one example of recent pioneering work in the field of liquid crystal science. Many other examples of fascinating research in novel areas to liquid crystal scientists are being explored. These include but are not limited to, research into the dynamic diffusion of smectic layers<sup>8</sup>, the production and mechanical properties of spider's silk<sup>9,10</sup>, the use of liquid crystalline systems to model biological materials and processes<sup>11</sup> and the dynamics of fluid filaments, films, foams, bubbles and nematic shells<sup>12-14</sup>.

One particularly interesting area of research is involved with the striking similarity that certain liquid crystalline phases can share with specific organic viruses. Interest in this area has spanned the lifetime of liquid crystal research, originating with characterisation of the Tobacco Mosaic virus in 1936<sup>15</sup>, through to cutting edge research on molecular permeation through smectic layers in a suspensions of 'rod like' viruses<sup>16-18</sup>. There is also an entirely new branch of soft matter photonics being developed, based on nematic colloids<sup>19</sup>, micro-lasers in liquid crystals<sup>20-22</sup> and optical trapping<sup>23,24</sup>.

That being said, there is still a wealth of interest and diversity within liquid crystal research, providing some of the most, in this author's opinion, interesting and often visually stimulating results. This introduction will now go on to give a brief outline of the content contained in the following chapters of this thesis.

### A. Thesis outline

A general introduction to the liquid crystalline phase of matter is given in Chapter 2, titled '*The liquid crystalline phase of matter*'.

Chapter 3, titled '*Theory / Methods*' examines the underlying theory required to understand the workings and output of the one dimensional model of nematic liquid crystals dynamics that is used extensively throughout this thesis. This chapter also examines the experimental methods (namely optical conoscopy and flow cell fabrication) used in order to make measurements of nematic liquid crystals undergoing pressure driven flow.

In Chapter 4, titled '*Flow alignment  $\phi_0 = 45^\circ$* ', a brief history of relevant flow experiments and processes is given before the results of a flow alignment experiment are presented, whereby optical conoscopy is used to mea-

## II INTRODUCTION

sure the mean azimuthal rotation of the director when it is initially aligned at an azimuth of  $45^\circ$  to the flow direction.

In Chapter 5, titled '*Uniform and splayed pretilt profiles*', the effect of surface pretilt on flow is experimentally investigated, with particular reference to the role of the two 'uniform' and 'splayed' alignment states that appear to lead to strikingly different director profiles when under flow. These experiments are conducted at an azimuthal angle close to normal to the flow direction.

Chapter 6, titled '*Producing intermediate surface pretilt*' examines experimental techniques and recipes for producing much larger pretilt angles of the director at the cell walls (as can be commercially desirable), presenting interesting experimental data from two such recipes, here measured using a novel high-throughput technique.

Finally, Chapter 7 titled '*Diode cell*' looks at the flow properties of a nematic liquid crystal exhibiting the large surface pretilt angles created using the research carried out in Chapter 6. Namely the idea of using a large pretilt angle in the 'splayed' state as a valve, introducing the 'diode' cell.

Chapter 8 then provides a summary and conclusion of the thesis, followed by a list of publications/presentations and bibliography.

### III. THE LIQUID CRYSTALLINE PHASE OF MATTER

As one may expect from the name, the *liquid crystalline* phase is a curious state of matter that lies somewhere between the *solid crystalline* and the *isotropic fluid* phases. As such, the liquid crystalline phase can exhibit extraordinary properties that belong to both the solid crystalline and isotropic fluid states of matter individually. For example, a liquid crystal can be shown to have the freedom to flow like any ordinary liquid (characteristic of the fluid phase) but also have the ability to exhibit birefringence (a characteristic of the solid crystalline phase). For such an exotic ‘fourth state of matter’, the term *mesophase* or *mesomorphic phase* is coined, meaning, quite simply, *intermediate phase*<sup>25</sup>.

Crudely speaking, all mesophases can be said to fall into one of two sub categories,

1. *Thermotropic* liquid crystals - the liquid crystalline mesophase occurs within a specific temperature range.
2. *Lyotropic* liquid crystals - the liquid crystalline mesophase occurs within a specific concentration range when dissolved in a solvent solution. Interestingly, many common materials show lyotropic behaviour, perhaps most importantly the bilayer membranes of living cells, where theories developed for liquid crystal physics have helped shed light on the effect of mitosis<sup>26</sup>. Perhaps less importantly, lyotropic materials are also mass produced for products such as shampoo and ice cream<sup>27</sup>.

Display devices, arguably the driving force behind the majority of liquid crystal research, are constructed solely from the thermotropic class of liquid crystal, and will therefore be the core study of this thesis.

#### A. Thermotropic liquid crystals

As is often the case when an area of science unites Physics, Chemistry and Biology, a multitude of classifications and labels are used to define subsets of materials. Liquid crystal classification is no different, and as such, the thermotropic class of liquid crystals can be further divided into the subdivisions of *Calamitic*, *Discotic* and *Polymeric*, where the division is made solely on the physical nature of the molecule comprising the liquid crystal phase.

- *Calamitic* liquid crystals are constructed from long, rod-like (uniaxial) molecules (see Figure 2). They exhibit a principal axis of orientation whereby the long molecular axes tend to align parallel to one another.
- *Discotic* liquid crystals are constructed from disc shaped molecules (one axis is significantly shorter

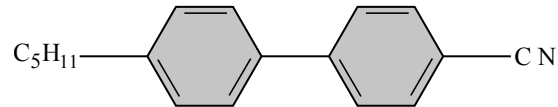


FIG. 2. The molecular structure of 5CB. With one long and 2 short axes, 5CB is a calamitic or ‘rod like’ material.

that the other two) and tend to align by stacking on top of each other like coins.

- *Polymeric* liquid crystals are constructed from long chain polymer molecules.

By far the majority of liquid crystal display devices are constructed from calamitic molecules, and through early work in the field, Friedel<sup>28</sup> was able to show that the calamitic class of molecule can be further divided into three separate sets, *Nematic*, *Smectic* and *Cholesteric* (see Figure 3). This time with the division made solely on the degree of order exhibited by the molecules in the phase.

- *Nematic* molecules possess three translational degrees of freedom and exhibit short-range orientational order whilst the molecular centres are distributed at random.
- *Smectic* molecules exhibit a positional order in at least one dimension, with the molecular centres on average arranged in equidistant planes<sup>29</sup>.
- *Cholesteric* molecules are very similar to those of the nematic class, but possess a twist in the direction of the short-range order as a function of position in the sample.

This classification system for mesophases and their molecule type is summarised by the flow chart in Figure 4.

#### B. Nematic liquid crystals

The main focus of the work in this thesis concerns the dynamic properties of nematic liquid crystals. As such, the features and properties that are key to understanding the nematic phase of thermotropic liquid crystals are summarised in the following paragraphs.

Firstly, included below are the three essential features exhibited by nematic phases,

- Nematic molecules will align, on average, with their long axes parallel to each other. Over macroscopic length scales, this alignment leads to a preferred direction in space, represented by the director  $\hat{n}$ . For almost all known thermotropic nematics, there exists rotational symmetry about  $\hat{n}$ .

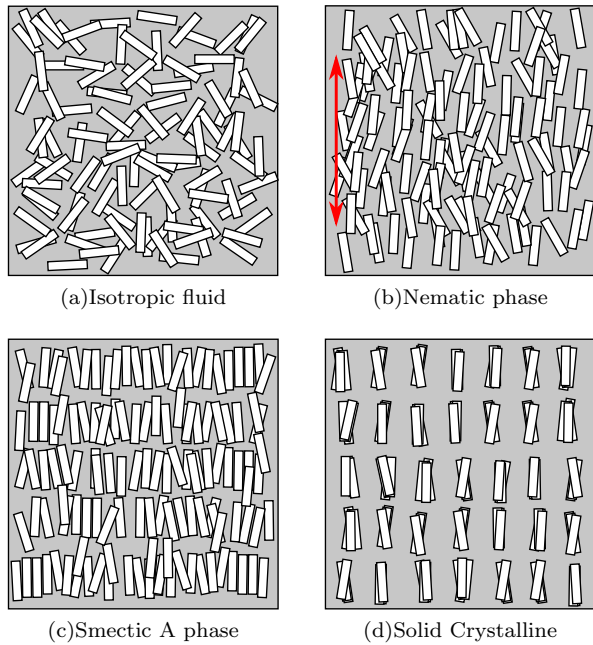


FIG. 3. Figures (a - d) depict schematic representations of the isotropic fluid, nematic, smectic and solid crystalline phases of matter. Each white rectangle represents an anisotropic molecule of the medium. The red arrow in (b) defines the average orientation of the molecules, known as the director.

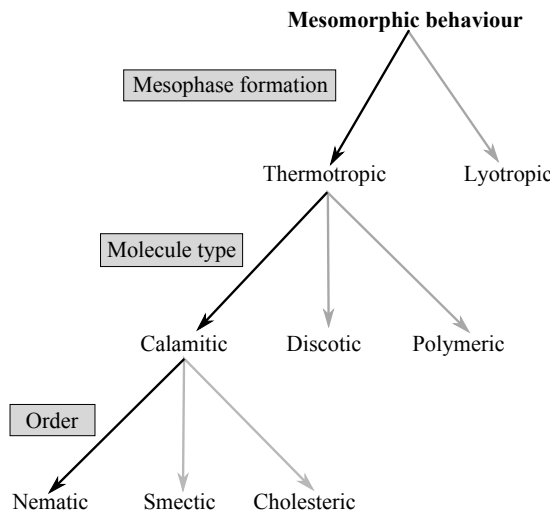


FIG. 4. A flow chart summarising the sub-divisions of mesophases and the criteria upon which the subdivisions are made (grey boxes).

- There is no correlation between the molecular centres of mass (no positional order). Hence the nematic phase is a fluid.
- There is no polarity associated with the uniaxial axis of symmetry ( $\hat{n} = -\hat{n}$ ).

### C. Nematic Order

The uniaxial, ‘rod like’ molecules of a nematic liquid crystal are defined to have an *ordinary* axis (denoted by a subscript *o*) with a length scale on the order of 5 Å, and an *extraordinary* axis (denoted by a subscript *e*) with a length scale on the order of 20 Å. In addition to the uniaxiality of nematics, as mentioned in Section III B, the nematic phase also exhibits a degree of short-range orientational order. Over macroscopic length scales, the orientation of individual molecules in a distribution will vary slightly, and importantly, this variation can be considered as time dependent, due to thermal fluctuations in the environment.

As such, the orientational order of a macroscopic sample is quantified by the order parameter, *s*, of the system, a quantity between *s* = 0 (random distribution of molecular orientations) and *s* = 1 (all molecules parallel to the director)<sup>4</sup>. The value of a system’s order parameter can be calculated from

$$s = \left\langle \frac{3}{2} \cos^2 \theta - \frac{1}{2} \right\rangle \quad (1)$$

where  $\theta$  is the angle between the individual molecule and the director, and the brackets denote an average taken over all molecules of the sample. In practice, the value of *s* is normally found to be around 0.3 or 0.4 at the clearing point,  $T_c$  (the transition temperature from the liquid crystal to isotropic fluid phase), and is found to be around 0.8 at much lower temperatures<sup>25</sup>.

### D. Optical Anisotropy

The uniaxial shape of a nematic molecule results in the refractive index associated with light polarised parallel to the director ( $n_e$ ) differing from that of light polarised perpendicular to the director ( $n_o$ ). This fundamental difference in the refractive indices is termed the *birefringence*, and is defined as

$$\Delta n = n_e - n_o \quad (2)$$

It is this birefringence that is exploited in all liquid crystal displays to produce contrast between picture elements. The values of  $n_o$  and  $n_e$  will differ with incident wavelength and also change as a function of temperature. For the liquid crystal 5CB at 25 °C and a wavelength

### III THE LIQUID CRYSTALLINE PHASE OF MATTER

of 633 nm, values of the refractive indices are close to  $n_o = 1.531$  and  $n_e = 1.706^{30}$ . Simply, if one considers a nematic liquid crystal sample where the temperature is being increased (and therefore through thermal fluctuations the order parameter is decreasing) it is easy to see that  $\Delta n$  will also decrease, and above  $T_c$  the refractive index is clearly single valued.

#### E. Dielectric Anisotropy

In direct parallel with the optical anisotropy, the dielectric permittivities are also directionally dependent, in association with the ordinary and extraordinary axes of the liquid crystal. The dielectric anisotropy is defined as,

$$\Delta\epsilon = \epsilon_e - \epsilon_o. \quad (3)$$

The value of  $\Delta\epsilon$  is responsible for dictating the reorientation of the director in response to an applied field. In the case of positive dielectric anisotropy ( $\epsilon_e > \epsilon_o$ ), the director will align parallel to the applied field lines. In the case of negative dielectric anisotropy ( $\epsilon_e < \epsilon_o$ ) the director will tend to align perpendicular to the field lines. It is this interaction between the reorientation of the director and the applied field, that is used to switch picture elements on and off in liquid crystal displays.

#### F. Elastic Constants and Free Energy

Due to spatial variations in the director, a nematic liquid crystal will always exhibit elastic free energy. When the director profile is confined between two aligning boundary layers, the molecules will reorientate to minimise the free energy per unit volume. As such, an appropriate free energy density  $w_f$  is defined by Frank and Oseen.

$$w_f = \frac{1}{2}k_{11}(\nabla \cdot \mathbf{n})^2 + \frac{1}{2}k_{22}(n \cdot \nabla \times \mathbf{n})^2 + \frac{1}{2}k_{33}|\mathbf{n} \times \nabla \times \mathbf{n}|^2 \quad (4)$$

Here, the constants  $k_{11}$ ,  $k_{22}$  and  $k_{33}$  correspond to the elastic deformations of the director field, splay, twist and bend, as are pictorially demonstrated in Figure 5. For typical nematic liquid crystals, the elastic constants have values on the order of  $10^{-11}$  N, which are obtained from experiments involving the competing effects of surface alignment and applied field alignment<sup>25</sup>. Typical values for the liquid crystal 5CB are given as  $k_{11} = 0.62 \times 10^{-11}$  N,  $k_{22} = 0.39 \times 10^{-11}$  N and  $k_{33} = 0.82 \times 10^{-11}$  N<sup>31</sup>. In the case of chiral nematics, a fourth term is added to the expression for the free energy density,

$$\frac{1}{2}(k_{22} + k_{24})\nabla \cdot (\mathbf{n} \cdot \nabla \mathbf{n} - \mathbf{n} \nabla \cdot \mathbf{n}) \quad (5)$$

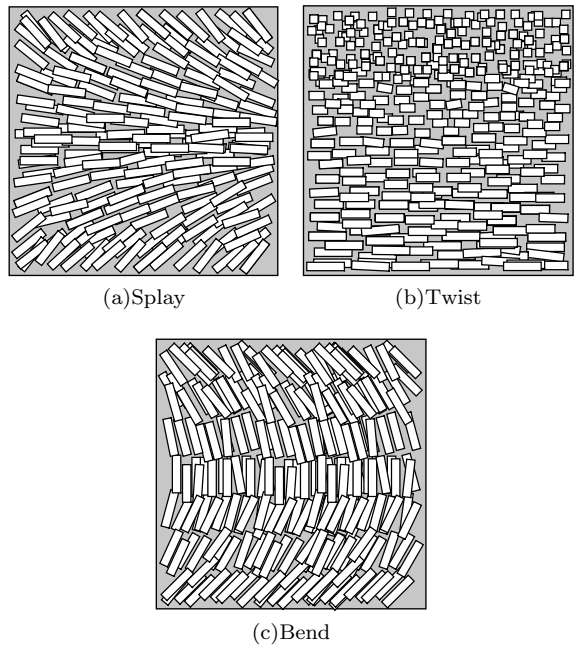


FIG. 5. A schematic diagram of the elastic deformations that can be imposed on a nematic liquid crystal via application of boundary conditions, (a) splay, (b) twist and (c) bend. Each white rectangle represents a nematic liquid crystal molecule. For the twist deformation (b), the director is rotating through  $90^\circ$  from the bottom surface to the top surface.

The free energy density expression for a non-chiral nematic does not include this term because the undistorted state is exactly the same as uniform alignment. The chirality of the molecules in a chiral nematic sample introduces an extra twist term between the intermolecular interactions.

#### G. Surface alignment

For efficient operation of nearly all liquid crystal devices, a well ordered and uniformly aligned mono-domain of the nematic director is required. In order to create uniform areas of alignment, the director can be forced to exhibit a specific direction relative to the cell wall by the application of a thin alignment layer, most commonly a spin-coated polyimide layer.

Commonly required alignments are for the director to be planar homogeneous (parallel to the surface, at any azimuthal angle), vertical (parallel to the surface-normal, also sometimes termed homeotropic alignment) and tilted alignment (any angle between planar and vertical). These alignment states are schematically depicted in Figure ?? (a), (b) and (c). It is also not uncommon to promote different alignment of the director on multiple surfaces of the same device. Such alignments can force large gradients in  $\hat{\mathbf{n}}$  in a stable state, thus creating non-

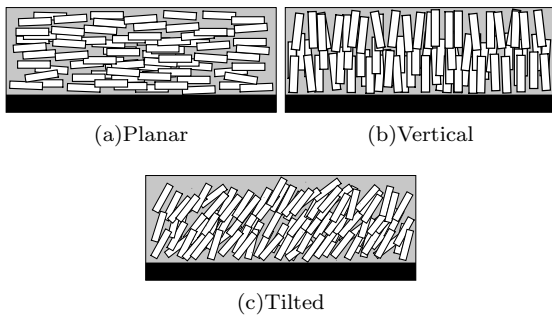


FIG. 6. Figures (a - c) depict schematic representations of planar, vertical and tilted alignment of the nematic director on a surface (black rectangle). Each white rectangle represents a nematic liquid crystal molecule.

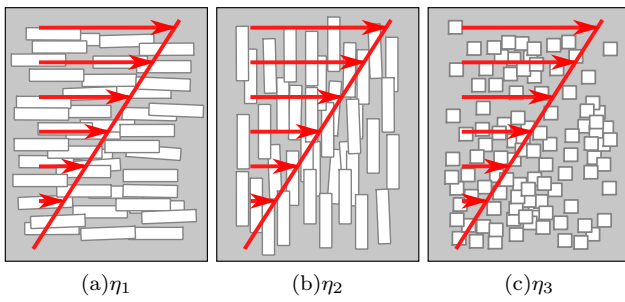


FIG. 7. A schematic diagram representing the relationship between the flow direction (red arrows) and the alignment of the director for the principal Miesowicz viscosities,  $\eta_1, \eta_2, \eta_3$ .

zero values of the free energy (equation 4). A much more detailed examination of surface alignment techniques and methods is discussed in Chapter ??.

## H. Nematic viscosities

Unlike regular isotropic fluids, nematic liquid crystals also exhibit anisotropic viscosity. That is, the viscosity (constant of proportionality between the applied shear stress and the induced velocity gradient) varies depending on the alignment of the director relative to the flow direction. The first accurate determination of these anisotropic viscosities in nematics was carried out by Professor Marian Miesowicz in the 1930s (originally published in a small bulletin in German), but was not reported wide-spread until after the war in 1946<sup>32</sup>. In his experiments, Miesowicz was able to distinguish three principal viscosity coefficients<sup>33</sup> ( $\eta_{1,2,3}$ ), shown schematically in Figure ?? through the application of a strong magnetic field used to align the director in different orientations relative to the flow direction.

As is shown in Figure ??, the three principal Miesowicz viscosities correspond to three orientations of the director

relative to the flow direction<sup>34</sup>,

1.  $\eta_1$  when  $\mathbf{n}$  is parallel to  $\mathbf{v}$
2.  $\eta_2$  when  $\mathbf{n}$  is parallel to  $\nabla\mathbf{v}$
3.  $\eta_3$  when  $\mathbf{n}$  is orthogonal to both  $\mathbf{v}$  and  $\nabla\mathbf{v}$

It is worth noting that as quoted in Janik's scientific appreciation of Miesowicz' work on the anisotropic viscosities of liquid crystals, '*...the accuracy of Miesowicz' experiments was so good that no significant improvement has been reported until the present time.*'<sup>35</sup>. The results of this experiment are perhaps made even more significant when one considers that during the 1930s it was a generally accepted paradigm that the properties of liquids were isotropic. As such, Miesowicz' results were originally met with some speculation from his contemporaries<sup>35</sup>. Values for the Miesowicz viscosities of 5CB near 25 °C are given as  $\eta_1 = 0.0204 \text{ Pa s}$ ,  $\eta_2 = 0.1052 \text{ Pa s}$ ,  $\eta_3 = 0.0326 \text{ Pa s}$ <sup>31</sup>.

As will be expanded upon in the next chapter, consideration of the full viscous stress tensor leads to the definition of not only the three principal Miesowicz viscosities as detailed above, but rather five independent viscosity coefficients for nematics. These viscosities cannot be related to the orientation of the director in a simple experimental manner<sup>31</sup> as is shown in Figure ?? but rather occur in linear combinations, making visualisation of nematic viscosities very difficult. As will be seen later, the five independent nematic viscosities can be mathematically related to the Miesowicz viscosities.

## IV. THEORY / METHODS

### A. Introduction

In this chapter, the theoretical background and one dimensional computational model (used to simulate the dynamic behaviour of nematic liquid crystals throughout this thesis) is discussed. This will begin with a brief look at the underlying equations and relations which ultimately lead to the one dimensional model and it's application in this research. The simulation of conoscopic figures based upon the director profiles obtained from the one dimensional model are also discussed. Finally, this chapter will look at the experimental methods for capturing conoscopic figures and the fabrication of bespoke cells allowing pressure driven flow from a syringe drive.

It should be noted that this chapter aims to give an introduction to the highly involved theoretical study of nematic liquid crystal dynamics, allowing insight into the results recorded in the experimental chapters to follow. Where relevant, references are provided to the original source material so that a deeper and fully exhaustive background can be obtained if desired.

### B. Background

At present (more than a century since the discovery of the liquid crystalline phase of matter), when studying the visco-elastic behaviour of nematic liquid crystals, the theory of Leslie and Ericksen is most frequently employed<sup>36</sup>. Along the road to arriving at this generally accepted and widely used theory, many different and wonderful ideas have been suggested regarding the nature and internal workings of nematic liquid crystals. Below, a brief description of the main historical milestones which lead to this formulation is given.

The first qualitative attempt at a descriptive model of liquid crystalline behaviour was made by Bose in the early 1900s. As is detailed in reference<sup>36</sup>, the core of his theory was based on the idea that the liquid crystalline phase of matter existed as small domains (of dimensions in the micron range) within which the director was assumed to remain constant. This idea was based on what was known at the time as *swarm theory*, a concept which dominated the theoretical modelling of liquid crystals for several decades<sup>36</sup>.

The first quantitative theory however, was presented by Born in 1916, where the existence of liquid crystalline phases was attributed to a permanent dipole attached to the molecules in the liquid<sup>36</sup>. Oseen was later able to show through a series of articles that Born's dipolar theory was wrong, whilst simultaneously describing a theoretical model for the static behaviour of liquid crystals which was essentially correct<sup>36</sup>. It was Anzelius, Oseen's student, who was then the first to publish an attempt at describing the dynamic behaviour of nematic liquid crystals, although unfortunately it was deemed to be in-

correct, despite several of its founding ideas being proven in retrospect to be sound<sup>36</sup>.

In the 1950s, along with the development of the modern theory of rational mechanics, a correct version of Anzelius's theory was finally established, resulting in the Leslie-Ericksen theory as it is known today<sup>36</sup> which is the mainstay of the theoretical description which follows in this chapter.

The following section goes on to introduce the Leslie-Ericksen theory in a form that is widely used today, starting from the constitutive equations and the definition of the dissipation function.

### C. Constitutive equations and the Leslie viscosities

Constitutive equations, or constitutive relations (reference<sup>31</sup> page 142), are expressions that provide a relationship between two physical quantities of a specific material or substance. In general, the constitutive equations provide a relationship between the response of a specific material and the forces applied to it. For the case of nematodynamics, the constitutive relationship considered links the rate of viscous dissipation (or, in an alternative but equivalent formulation, the stress tensor) and the motion of the liquid crystal. It is important to note here that constitutive equations are used to describe the mechanical properties *particular to a given medium* and will thus change from one medium to another.

As is described by Stewart<sup>31</sup>, the natural continuum variables to consider for constitutive equations governing the dynamics of nematic liquid crystals are those of the director, the local angular velocity of the director and the pressure-induced velocity gradients within the medium. Analogously to the Frank equation which relates the free energy density  $\omega_f$  (equation 4), to gradients in  $\mathbf{n}$ , one can relate the rate of viscous dissipation to director rotations and spatial variations in the fluid velocity. Following from Leslie's<sup>37</sup> formulation, this equation is obtained from a '*rate of work hypothesis*', which makes the following assumption;

*"The rate at which forces and moments do work on a volume of nematic will be absorbed into changes in the nematic energy ( $\omega_f$ ) or the kinetic energy, or will be lost by means of viscous dissipation"*<sup>31</sup>.

As is the case for any classically based continuum theory (where isothermal conditions are assumed, and therefore thermal effects are ignored), conservation laws of mass, linear momentum and angular momentum must hold. Therefore, for a volume  $V$  of nematic liquid crystal bounded by the surface  $S$ , this rate of work postulate can mathematically be described as

$$\int_V \rho (\mathbf{F} \cdot \mathbf{v} + \mathbf{K} \cdot \mathbf{w}) dV + \int_S (\mathbf{t} \cdot \mathbf{v} + \mathbf{l} \cdot \mathbf{w}) dS = \frac{D}{Dt} \int_V \left( \frac{1}{2} \rho \mathbf{v} \cdot \mathbf{v} + \omega_f \right) dV \quad (6)$$

where  $\rho$  denotes the density,  $\mathbf{F}$  is the external body force per unit mass,  $\mathbf{v}$  is the velocity,  $\mathbf{K}$  is the external body moment per unit mass,  $\mathbf{w}$  is the local angular velocity of the director,  $\mathbf{t}$  is the surface force per unit area,  $\mathbf{l}$  is the surface moment per unit area and  $\mathcal{D}$  signifies the rate of viscous dissipation per unit volume (known as the **dissipation function**).

Following from the rigorous derivation provided by Stewart<sup>31</sup>, the dissipation function  $\mathcal{D}$  (through the balance laws for mass, linear momentum and angular momentum) can be expressed as<sup>38</sup>

$$\mathcal{D} = \alpha_1 (n_i A_{ij} n_j)^2 + 2(\alpha_2 + \alpha_3) N_i A_{ij} n_j + \alpha_4 A_{ij} A_{ij} + (\alpha_5 + \alpha_6) n_i A_{ij} A_{jk} n_k + (\alpha_3 - \alpha_2) N_i N_i \geq 0 \quad (7)$$

where the coefficients  $\alpha_1, \alpha_2, \dots, \alpha_6$  are known as the *Leslie viscosity coefficients, or the Leslie viscosities*,  $n_{i,j}$  is the director,  $A$  is the rate of strain tensor given by

$$A_{ij} = \frac{1}{2} (v_{i,j} + v_{j,i}) \quad (8)$$

and  $N_i$  is the co-rotational time flux of the director given by

$$N_i = \dot{n}_i - W_{ij} n_j \quad (9)$$

where  $W_{ij}$  is the vorticity tensor, given by

$$W_{ij} = \frac{1}{2} (v_{i,j} - v_{j,i}) \quad (10)$$

Importantly, there are, of course, many combinations in the constitutive relation with regards to the continuum variables that result in the dissipation of energy under flow. Thankfully, much like in the case of the Frank free energy relation, the consideration of nematic constraints such as the equivalence of  $\mathbf{n}$  and  $-\mathbf{n}$  and the fact that the constitutive relations must be invariant under reflections within planes containing  $\mathbf{n}$  (due to the symmetry of nematic liquid crystals), **these combinations reduce to just the six Leslie viscosities** (in much the same way that the Frank free energy reduces to the primary splay, twist and bend elastic constants).

As can be seen by the inequality shown in equation 7,  $\mathcal{D}$  is always constrained to be positive. This seems appropriate, as we expect any system to *lose* energy through the viscous dissipation due to spatial variations in the velocity profile.

#### D. Comments and Constraints on the Leslie viscosities

In the previous section (IV C), six independent viscosity coefficients have been introduced (a full description

of which is provided in reference<sup>31</sup>), through the dissipation function, to exist for standard rod-like nematic liquid crystals. However, unlike the case of the previously described Miesowicz viscosities (Figure ??), where only three viscosity coefficients are considered (based on the alignment of the director with respect to the shear flow), one cannot formulate an intuitive understanding of the relationship between the director and the flow direction in order to gain an understanding of the six individual Leslie viscosity's contribution to a nematic liquid crystal under flow.

Thankfully, from a simple analysis of the terms comprising the dissipation function, it is possible to gain substantial insight into the relative importance and physical contribution from some of the Leslie viscosity coefficients. For example, equation 7 shows that the only term containing the Leslie viscosity  $\alpha_4$ , does not contain any terms relating to the director ( $n, N$ ), but rather only contains the rate of strain tensor  $A$ . Therefore,  $\alpha_4$  is often considered to be the analogue of the isotropic viscosity coefficient, in that its value is not affected by the relative director orientation. Similarly, the only terms in equation 7 that contain the co-rotational time flux of the director  $N$ , are terms solely containing the Leslie viscosities  $\alpha_2$  and  $\alpha_3$ . Therefore, the Leslie viscosities associated with the rotation of the director are predominantly  $\alpha_2$  and  $\alpha_3$ , where  $\gamma_1 = \alpha_3 - \alpha_2$ , and is often termed the rotational or Tsvetkov's viscosity coefficient<sup>39</sup>. The role of  $\alpha_2$  and  $\alpha_3$  on director rotation will be expanded upon in later sections.

Much like the Frank elastic constants, the Leslie viscosities are phenomenological, meaning that their values are not derived from first principles. In fact, as the Leslie viscosities do not correlate to simple physical geometries (as is the case for the Miesowicz viscosity coefficients), they cannot be directly measured. Rather, combinations of the Leslie viscosities are measured. Be this as it may, it can be shown that the values of the Leslie viscosities are constrained by the second law of thermodynamics, which results in a set of inequalities governing their sign. These inequalities<sup>31</sup> are defined below for convenience, as some of them will be used later in further analysis of the dynamic theory.

$$\gamma_1 = \alpha_3 - \alpha_2 \geq 0 \quad (11)$$

$$\alpha_4 \geq 0 \quad (12)$$

$$2\alpha_4 + \alpha_5 + \alpha_6 \geq 0 \quad (13)$$

$$2\alpha_1 + 3\alpha_4 + 2\alpha_5 + 2\alpha_6 \geq 0 \quad (14)$$

$$4\gamma_1 (2\alpha_4 + \alpha_5 + \alpha_6) \geq (\alpha_2 + \alpha_3 + \gamma_2)^2 \quad (15)$$

From these inequalities, it is important to note that the rotational viscosity  $\gamma_1$  must have a positive value, as must  $\alpha_4$ , the analogue of the isotropic viscosity coefficient. For reference, the Miesowicz viscosity coefficients are related to the Leslie viscosity coefficients and can be converted via the relations given in Table I. Here it is plain to see the

Viscosity conversions	
Leslie to Miesowicz	Miesowicz to Leslie
$\alpha_1 = \eta_{12}$	$\eta_1 = (\alpha_2 + 2\alpha_3 + \alpha_4 + \alpha_5)$
$\alpha_2 = \frac{1}{2}(\eta_1 - \eta_2 - \gamma_1)$	$\eta_2 = \frac{1}{2}(-\alpha_2 + \alpha_4 + \alpha_5)$
$\alpha_3 = \frac{1}{2}(\eta_1 - \eta_2 + \gamma_1)$	$\eta_3 = \frac{1}{2}\alpha_4$
$\alpha_4 = 2\eta_3$	$\eta_{12} = \alpha_1$
$\alpha_5 = \frac{1}{2}(\eta_1 + 3\eta_2 - 4\eta_3 - \gamma_1)$	
$\alpha_6 = \alpha_2 + \alpha_3 + \alpha_5$	

TABLE I. A table providing a summary of the relationships that link the Leslie viscosities to the Miesowicz viscosities and *vice versa*.

somewhat complex relationships between the Miesowicz and Leslie viscosities.

### E. The Parodi relation

In 1970, Parodi<sup>40</sup> proposed, through Onsager relations, that **there are in fact only five independent viscosity coefficients** that need to be considered. This result often leads to simplifications in the theoretical analysis which makes for far easier computation. The relation,

$$\alpha_6 - \alpha_5 = \alpha_2 + \alpha_3 = \gamma_2 \quad (16)$$

was verified by Currie<sup>41</sup> in 1974, and is a generally accepted addition to the Leslie-Ericksen theory, which is sometimes termed the Leslie-Ericksen-Parodi (LEP) theory of nematic liquid crystals.

### F. Flow-alignment (“logs in rivers”)

As is carried through the rest of this thesis, the Euler angles  $\theta(z, t)$  and  $\phi(z, t)$  are used to specify the director  $\mathbf{n}$ . Here, as is traditional in the Exeter group, the tilt angle  $\theta$  is defined to be measured from the  $z$  axis and the twist angle  $\phi$  is defined to be the angle between the projection of  $\mathbf{n}$  on to the  $x - y$  plane and the  $x$  axis. The flow direction throughout this thesis is also defined to be in the positive  $x$  direction, with the gradient in velocity in the  $z$  direction as also shown in Figure 8.

In this section, the theory of nematic liquid crystal *flow-alignment* is introduced. That is, the response of the director  $\mathbf{n}$  to a velocity gradient. However, to begin with, it is pertinent to pose the question, “*How do we intuitively expect the nematic director to respond to a velocity field?*”

In order to answer this question, a simplified picture of nematic liquid crystal molecules under flow is introduced. This is done by firstly imagining that rather than having molecules flowing in a well defined channel, we replace the channel walls with river banks, and secondly by imagining that rather than having rod-like liquid crystalline molecules, we replace them with wooden logs. If one pictures the flow of a nematic liquid crystal as being

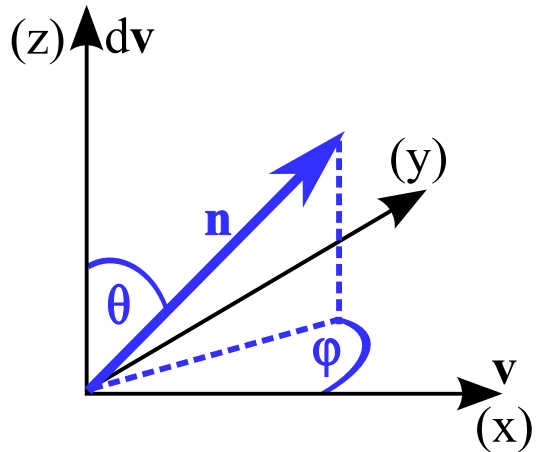


FIG. 8. Coordinate system used throughout this thesis. The tilt angle  $\theta$  is defined to be measured from the  $z$  axis and the twist angle  $\phi$  is defined to be the angle between the projection of  $\mathbf{n}$  on to the  $x - y$  plane and the  $x$  axis



FIG. 9. ‘Timber being floated to Vancouver, Canada’. This photograph illustrates how the idea of logs in a river can greatly aid the visualisation of nematic flow-alignment. Here, individual logs are considered the analogue of calamitic liquid crystal molecules, with one long and two short axes. The photograph is licensed under the Creative Commons Attribution 2.0 Generic license and can be found at [http://en.wikipedia.org/wiki/File:Log\\_driving\\_in\\_Vancouver.jpg](http://en.wikipedia.org/wiki/File:Log_driving_in_Vancouver.jpg)

directly analogous to the flow of logs in a river (Figure 9), a simple, intuitive and useful picture can be formulated in the reader’s mind, which will help during later stages in visualising the director’s response under complex flow geometries.

It is clear that the three Miesowicz viscosity geometries pictured in Figure ?? can equally be represented by wooden logs flowing in Figure 9. This could be achieved by constraining the logs to have specific orientations with respect to the river velocity and river velocity gradient. Here, the orientation shown in Figure 9 is equivalent to

that of  $\eta_1$ , where  $\mathbf{n} \parallel v$ .

Perhaps intuitively one may expect the director, in response to flow, to azimuthally align itself parallel to the flow direction, as is depicted in Figure 9. It seems natural to assume that logs in a river will flow *more easily* in this orientation ( $\phi = 0^\circ$ ). As for the zenithal orientation of the director, again, flow with the logs in planar alignment ( $\theta = 90^\circ$ ) (as in Figure 9) naturally feels to be the orientation under which the logs will flow most easily.

As we shall see in the next section, this simplified picture is not entirely incorrect, particularly with respect to the preferred azimuthal orientation of  $\phi = 0^\circ$ , providing a very intuitive picture to refer to when analysing more complex flow geometries. Perhaps most interestingly, it will also be shown that for a certain class of liquid crystal, a tilt angle of  $\theta = 90^\circ$  is not the preferred orientation under flow, but that it is rather some small angle away from planar, at which point, the net viscous torque on the nematic molecules goes to zero.

### G. Simplified flow-alignment

In order to gain a basic understanding of the nematic director's response to a flow field, a highly simplified, and in some respects, unrealistic scenario is considered. In this scenario, all effects of boundaries, external fields, director gradients and elastic energies are ignored, leaving only the influence of a linear velocity gradient in  $z$  to be considered.

For such a simplified system, the Ericksen-Leslie dynamic equations reduce to two equations, governing the time derivative of  $\theta$ , ( $\dot{\theta} = d\theta/dt$ ) and the time derivative of  $\phi$ , ( $\dot{\phi} = d\phi/dt$ )<sup>31</sup>. These equations describe the orientation of  $\mathbf{n}$  for the simplest of shear flow regimes, which apply strictly only under the conditions stated above. These equations are given below (17 and 18).

$$\gamma_1 \dot{\theta} = k (\alpha_3 \sin^2 \theta - \alpha_2 \cos^2 \theta) \cos \phi \quad (17)$$

$$\gamma_1 \cos \theta \dot{\phi} = k \alpha_3 \sin \theta \sin \phi \quad (18)$$

As explained by Stewart<sup>31</sup>, it is natural to then proceed by seeking steady state solutions to both equations 17 and 18. That is to ask, “*what values of  $\theta$  and  $\phi$  are the steady values under shear flow?*” This question is answered by setting  $\dot{\theta} = \dot{\phi} = 0$ , i.e. solving both equations in the condition that the director has stopped rotating, or achieved steady state alignment.

Therefore it is seen that for any values of the viscosities (bearing in mind the equivalence of  $\mathbf{n}$  and  $-\mathbf{n}$ , there is always the steady state alignment provided by

$$\theta = 90^\circ, \quad \phi = 90^\circ \quad (19)$$

These steady state alignment angles correspond to the director being planar ( $\theta = 90^\circ$ ), and lying normal to the

flow direction ( $\phi = 90^\circ$ ), as depicted in Figure 10 (a). Intuitively, this stable alignment condition makes sense. If there is no component of the director in the  $z$  direction, then there is no torque acting on the molecules, and therefore there is no torque imbalance, leading to a steady state alignment angle. For a nematic liquid crystal oriented normal to the flow and planar, there is no rotation of the director caused by a shear flow.

However, it can be seen that if the Leslie viscosities  $\alpha_2$  and  $\alpha_3$  are non-zero and have the same sign, such that  $\alpha_2 \alpha_3 > 0$ , other possible steady state solutions are provided by

$$\theta = \theta_l, \quad \phi = 0^\circ \quad (20)$$

where the angle  $\theta_l$  is referred to as the Leslie angle or *flow alignment angle*, and is calculated from equation 21, below.

$$\alpha_3 \sin^2 \theta = \alpha_2 \cos^2 \theta$$

$$\tan^2 \theta = \frac{\alpha_2}{\alpha_3}$$

$$\theta = \tan^{-1} \sqrt{\alpha_2/\alpha_3} \quad (21)$$

$$\theta_l = 90^\circ - \theta \quad (22)$$

Note that the Leslie angle is conventionally defined as a deviation out of the  $x - y$  plane, hence the inclusion of equation 22 to convert our angle into the conventional form. Now it is seen that there is a second set of steady state alignment angles for the director. These constrain the director to be aligned parallel to the direction of flow ( $\phi = 0^\circ$ ), but crucially, not planar aligned ( $\theta \neq 90^\circ$ ), but at some small angle ( $90^\circ - \theta_l$ ) away from planar, as is demonstrated in Figure 10 (b).

Importantly, if the values of  $\alpha_2$  and  $\alpha_3$  differ in sign, the only steady state solutions under flow are those given by equation 19. This follows from equation 21, where the steady state alignment angle for  $\theta$  would involve the square-root of a negative number. Therefore, two classes of liquid crystal can be defined.

- *Flow-aligning* liquid crystals; where  $\alpha_2 \alpha_3 > 0$
- *Non flow-aligning* liquid crystals; where  $\alpha_2 \alpha_3 < 0$

It follows that for flow-aligning liquid crystals, there are two further sub-categories which depend on the relative strengths of  $\alpha_2$  and  $\alpha_3$ , which comes from the thermodynamic constraint that  $\gamma_1 = \alpha_3 - \alpha_2 > 0$ , defined by,

$$\text{Type I } \alpha_2 < \alpha_3 < 0 \quad \text{where} \quad 0^\circ < \theta_l < 45^\circ, \quad \phi = 0^\circ \quad (23)$$

$$\text{Type II } \alpha_3 > \alpha_2 > 0 \quad \text{where} \quad 45^\circ < \theta_l < 90^\circ, \quad \phi = 0^\circ \quad (24)$$

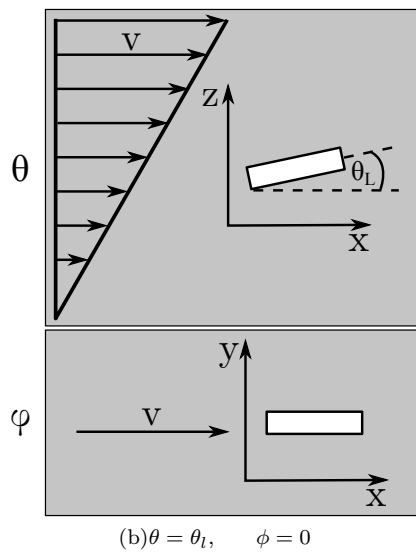
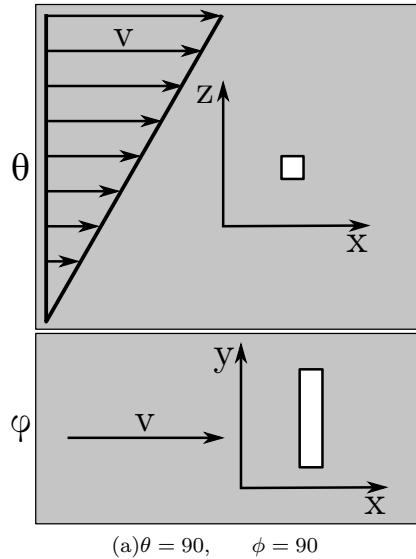


FIG. 10. Visual schematic depictions of the steady state alignment angles available to the director under a highly simplified shear flow. (a) shows the alignment angles of  $\theta = 90^\circ$  and  $\phi = 90^\circ$ , which are available for any values of the Leslie viscosities. (b) shows the alignment angles of  $\theta = \theta_l$  and  $\phi = 0^\circ$ , which are only available for *flow-aligning* liquid crystals ( $\alpha_2\alpha_3 > 0$ ).

Here we see that for  $\alpha_2 < \alpha_3 < 0$ , the steady state Leslie angle will be valued somewhere between  $\theta = 90^\circ$  and  $\theta = 45^\circ$ , which is a relatively small angular deviation away from planar alignment. Conversely, in the case of  $\alpha_3 < \alpha_2 > 0$ , the Leslie angle will be valued between  $\theta = 45^\circ$  and  $\theta = 0^\circ$ , which is a relatively large distortion away from planar alignment. It is purely this torque balance, created by the differing relative strengths of  $\alpha_2$  and  $\alpha_3$  which create the steady state Leslie angle.

The values of the Leslie viscosity coefficients for three common nematic liquid crystals are given in Table II.

It can be seen for the experimental viscosities given in Table II, that 5CB, MBBA and PAA are all Type I *flow-aligning*.

Liquid Crystal	T °C	Leslie Viscosity (Pa.s)					
		$\alpha_1$	$\alpha_2$	$\alpha_3$	$\alpha_4$	$\alpha_5$	$\alpha_6$
5CB	25°	-0.0060	-0.0812	-0.0036	0.0652	0.0640	-0.0208
MBBA	25°	-0.0181	-0.1104	-0.0011	0.0826	0.0779	-0.0336
PAA	122°	0.0043	-0.0069	-0.0002	0.0068	0.0047	-0.0023

TABLE II. Values of the Leslie viscosities for the nematic phases of 5CB, MBBA and PAA (taken from reference<sup>31</sup>). Note that all three nematic phases are flow-aligning.

After this introduction to the theoretical background of nematic liquid crystal dynamics, this chapter will now go on to introduce and examine the workings of the one dimensional model that is used to simulate director dynamics in liquid crystal cells undergoing pressure driven flow in well defined flow channels.

## H. A 1-D numerical model of liquid crystal dynamics

This section introduces the one dimensional model of liquid crystal dynamics that is used extensively in later chapters of this thesis. The rigorous and full details of the model's design and operation are provided by its creator, Stephen Cornford, in his thesis "Recovery and analysis of director profiles in liquid crystal cells"<sup>42</sup> where a substantial amount of effort has gone into creating the model and comparing its output to other simulation packages available (such as DIMOS). As is described in reference<sup>42</sup>, although other computer programs that can model simple liquid crystal cells have been used before in the Exeter group<sup>43,44</sup>, this model was created in order to compute the dynamics of rather more complex situations including simulation of the flexo-electric effect, ion motion in cells, use in optimisation problems and, most importantly in the context of this thesis, the effects of pressure-driven flow upon director distortion.

This section aims to provide a brief introduction to the key equations of the model which govern the dynamic behaviour that will be seen in later experimental chapters of this thesis. In addition to that, this section also intends to give a brief introduction to how the model is used in this thesis, including what difficulties have been overcome in order for it to operate.

### 1. Assumptions

The dynamical behaviour of the liquid crystal described by this one dimensional model is governed by the Leslie-Ericksen equations (as introduced earlier in this chapter). That is to say, the model is derived from the continuum theory of nematic liquid crystals, where the liquid crystal is described by a director field<sup>42</sup>.

For a simple cell, the liquid crystal can be described by this director field  $\mathbf{n}(z, t)$ , and a flow field  $\mathbf{u}(z, t)$ . Given this assumption, the model is based upon a Cartesian co-ordinate system that has been chosen so the cell walls (upper and lower) lie parallel to the  $xy$  plane at  $z = 0$  and  $z = d$ . As this is only a one dimensional simulation, the cell is also assumed to be infinitely large in both the  $x$  and  $y$  directions so that only variations in the director parallel to the  $z$  axis need to be considered<sup>42</sup>. As was described at the start of Section IV F (Figure 8), the Euler angles  $\theta(z, t)$  and  $\phi(z, t)$  are used to specify the director  $\mathbf{n}$ . As is traditional in the Exeter group, the tilt angle  $\theta$  is defined to be measured from the  $z$  axis and the twist angle  $\phi$  is defined to be the angle between the projection of  $\mathbf{n}$  on to the  $x - y$  plane and the  $x$  axis, expressed as

$$\mathbf{n} = (\sin \theta \cos \phi, \sin \theta \sin \phi, \cos \theta) \quad (25)$$

Another result of the one dimensional assumption is that only two variables  $u_x$  and  $u_y$  are needed to fully

describe the nature of  $\mathbf{u}$ . As is detailed in<sup>42</sup> the basis for this assumption is made clear when  $\mathbf{u}$  is taken to be defined by

$$\mathbf{u} = (u_x, u_y, u_z) \quad (26)$$

As the flow is assumed to be incompressible,  $\nabla \cdot \mathbf{u} = 0$ . If the flow field *varies* only in  $z$ , this divergence equality reduces to

$$\frac{\partial u_z}{\partial z} = 0 \quad (27)$$

Since there is no flow through the top and bottom walls of the cell,  $u_z(0) = u_z(d) = 0$ , and therefore  $u_z$  must equal zero, and hence there is only the requirement for two variables  $u_x$  and  $u_y$  to fully describe  $\mathbf{u}$ .

It is worth noting that as well as the director and flow fields described above, the electric field  $\mathbf{E}$  within the cell must be taken into account if simulations involving the effects of an applied electric potential are also to be considered<sup>45</sup>. In such a case, the electric displacement vector  $\mathbf{D}$ , must be constant in a one dimensional system<sup>42</sup>. As  $\mathbf{D}$  is confined to be parallel to the  $z$  axis at the cell boundaries, it must therefore be parallel to  $z$  at all points in the cell and hence only components of  $\mathbf{E}$  parallel to the  $z$  axis are considered in the simulation equations.

## I. The Leslie-Ericksen equations

The time and space dependent behaviour of  $\mathbf{n}$  and  $\mathbf{u}$  can be found by solving the Leslie-Ericksen equations. These equations boil down to four partial differential equations in the variables  $\theta, \phi, u_x$  and  $u_y$ . Prior to examining these equations, some auxiliary functions of  $\theta$  are defined for convenience<sup>42</sup>

$$a(\theta) = (\alpha_6 + \alpha_3 + 2\alpha_1 \cos^2 \theta) \sin^2 \theta \quad (28)$$

$$b(\theta) = (\alpha_5 - \alpha_2) \cos^2 \theta + \alpha_4 \quad (29)$$

$$c(\theta) = \alpha_3 \sin^2 \theta - \alpha_2 \cos^2 \theta \quad (30)$$

$$g(\theta) = \sin^2 \theta ((k_{22} - k_{33}) \sin^2 \theta + k_{33}) \quad (31)$$

$$g'(\theta) = \frac{dg}{d\theta} \quad (32)$$

## J. Twist

The governing equation for the azimuthal angle  $\phi$  is derived from<sup>42</sup> and<sup>31</sup>,

$$\gamma_1 \sin^2 \theta \frac{d\phi}{dt} = g(\theta) \frac{\partial^2 \phi}{\partial z^2} + g'(\theta) \frac{\partial \theta}{\partial z} \frac{\partial \phi}{\partial z} - \frac{1}{2} \alpha_2 \sin 2\theta \left( \cos \phi \frac{\partial u_y}{\partial z} - \sin \phi \frac{\partial u_x}{\partial z} \right) \quad (33)$$

Boundary conditions and initial conditions for equation 33 must be provided, giving  $\phi(z = 0, t = 0)$ ,  $\phi(z = d, t = 0)$  and  $\theta(z, t = 0)$ . That is, the initial azimuthal director alignment has to be provided. Generally, when simulating the response of a cell, the angles in the simulation will be those of the rubbing direction on the actual cell.

If a uniform ( $d\phi/dz = 0$ ), planar aligned ( $\theta = 90^\circ$ ) sample were to be considered, it is seen that all terms in equation 33 equal zero. That is to say, if a liquid crystal sample were to be held planar, there would be no azimuthal distortion of the director under flow (the same is also true for  $\theta = 0^\circ$ ). However, if there were to be a small amount of tilt of the director introduced to the cell ( $\theta \neq 90^\circ$ ), the third term in equation 33,

$$\frac{1}{2}\alpha_2 \sin 2\theta \left( \cos \phi \frac{\partial u_y}{\partial z} - \sin \phi \frac{\partial u_x}{\partial z} \right) \quad (34)$$

will no longer equal zero, and azimuthal rotation of the director will be simulated with the onset of flow. This result is important, and ties in with the more qualitative explanation of azimuthal rotation which is described later in Chapter ??.

Another important point to note about equation 33 is that in steady state, where  $d\phi/dt = 0$ , (ignoring the contribution from  $u_y \sin \phi (\partial u_x/\partial z)$  in the final term) must also equal zero. Given that under flow  $\partial u_x/\partial z$  will not equal zero, then the value of  $\sin \phi$  must equal zero, yielding steady state values of  $\phi = 0^\circ, 180^\circ$ , or the director lying parallel to the  $x$  axis (flow direction). Therefore, considering the more involved equations describing the dynamic behaviour of a nematic liquid crystal under pressure driven flow between two parallel plates, the same steady state azimuthal alignment angles of the director are recovered, as were seen earlier for the highly simplified case in the azimuthal component of equation 20.

## K. Tilt

A similar governing equation for the zenithal (tilt) angle  $\theta$  is derived from<sup>42</sup> and<sup>31</sup>,

$$\begin{aligned} \gamma_1 \frac{\partial \theta}{\partial t} &= (k_{11} + (k_{33} - k_{11}) \cos^2 \theta) \frac{\partial^2 \theta}{\partial z^2} \\ &+ \frac{1}{2} (k_{11} - k_{33}) \sin 2\theta \left( \frac{\partial \theta}{\partial z} \right)^2 \\ &+ \frac{1}{2} g'(\theta) \left( \frac{\partial \phi}{\partial z} \right)^2 + c(\theta) \left( \cos \phi \frac{\partial u_x}{\partial z} + \sin \phi \frac{\partial u_y}{\partial z} \right) \\ &+ \frac{1}{2} \sin 2\theta \left( (e_s - e_b) \frac{\partial E}{\partial z} - \epsilon_0 \epsilon_a E^2 \right) \end{aligned} \quad (35)$$

Again, boundary conditions for equation 35 must be provided, giving  $\theta(z = 0, t = 0)$ ,  $\theta(z = d, t = 0)$  and

$\theta(z, t = 0)$ . That is, the initial tilt director alignment has to be provided, again, this is provided physically by the type of surface alignment layer that is deposited on cell walls.

Here, in steady state and assuming a uniform alignment ( $\partial \theta/\partial t = 0$ ),  $c(\theta)$  must equal zero, which from equation 21 is shown to occur at the Leslie angle.

## L. Flow field

The last two governing equations are those for the simulated flow field and are derived from the linear momentum balance equations<sup>42</sup> where the pressure gradients  $G_x$  and  $G_y$  are defined along the  $x$  and  $y$  axes respectively. These are given in 36 and 37 below.

It is worth noting that the only time derivatives contained in equations 36 and 37 are those of  $\theta$  and  $\phi$ . This dictates that if the director is not changing in time, the flow fields are also time independent. Consequently, only boundary conditions for  $u_x$  and  $u_y$  must be prescribed. As will also be discussed later, the classical non-slip boundary condition stating that the fluid velocity at the cell walls is assumed to be zero is appropriate<sup>42,46</sup>.

$$G_x = \frac{\partial}{\partial z} \left( \left[ \frac{1}{2} a(\theta) \cos^2 \phi + b(\theta) \right] \frac{\partial u_x}{\partial z} + \frac{1}{4} a(\theta) \sin 2\phi \frac{\partial u_y}{\partial z} - c(\theta) \cos \phi \right) \quad (36)$$

$$G_y = \frac{\partial}{\partial z} \left( \left[ \frac{1}{2} a(\theta) \sin^2 \phi + b(\theta) \right] \frac{\partial u_y}{\partial z} + \frac{1}{4} a(\theta) \sin 2\phi \frac{\partial u_x}{\partial z} - c(\theta) \sin \phi \right) \quad (37)$$

As a final note, as discussed earlier and shown in equations 33 and 35, the boundary conditions for  $\theta$  and  $\phi$  are known (from experiment) and are input into the one dimensional model used here. As is explained in<sup>42</sup>, it is also reasonable to assume that the director is fixed at the cell surfaces, in a regime known as *strong anchoring*. An alternative regime could also be considered, *weak anchoring* (not used in this simulation) whereby information regarding  $\theta$  and its derivative in  $z$  and  $\phi$  and its derivative in  $z$  would be required<sup>47</sup>.

Finally, this chapter will go on to introduce the experimental technique of conoscopy as a means of extracting information about nematic liquid crystal alignment. Conoscopy is used widely in later experimental chapters of this thesis and here, a computational method of simulating conoscopic figures is introduced along with some characteristic figures recorded in the experiments.

### M. Conoscopy

Conoscopy, from the greek *konos* meaning cone, and *skopeo* meaning examine<sup>48</sup>, has long been used as a tool for studying the physical nature and alignment of geological crystals and their birefringence. More recently, it has been used to explore liquid crystal mono-domain alignment<sup>49</sup>. As will be seen later in the experimental chapters of this thesis, conoscopy is also a relatively simple and powerful tool for gaining a large amount of information about a liquid crystal director profile in a relatively quick manner. Not notwithstanding it's relative speed-of-use and ease of implementation, it does have certain shortcomings when directly compared to more detailed and rigorous analysis methods such as the Fully Leaky Guided Mode (FLGM) technique<sup>50-54</sup>.

Optical conoscopy, as used in this work, gives a broad (lacking in fine detail) picture of how the director behaves or reacts to an external perturbation such as an applied pressure gradient inducing flow. As such, the aim of conoscopy is not to accurately determine the director profile at a high spatial resolution, but rather to give a broad overview of the alignment present within the cell.

### N. Simulation

Conoscopic ‘interference’ figures are generated when birefringent crystal samples are viewed between crossed polarisers with highly convergent monochromatic light<sup>55</sup>. Essentially, as is well explained by Van Horn and Henning-Winter<sup>49</sup>, when light rays pass through the crystal, they are split into ordinary and extraordinary components which experience different refractive indices and hence travel along different paths. For liquid crystal mono-domains, these different paths are highly dependent on the degree of order exhibited within the liquid crystal mono-domain. Depending on the phase difference between these rays, light exiting the crystal may have undergone polarisation conversion, resulting in some light in specific directions passing the second, crossed, polariser. For light rays over a cone of angles, characteristic figures are observed, depending on the alignment of the mono-domain that has been traversed.

Figure 11 shows a schematic representation of the common conoscopic figures that are observed for the primary alignment states of the director. For reference, conoscopic figures are said to consist of dark isochromatic fringes, and extinction brushes or *isogyres*. When the director is aligned parallel to the surface (planar, Figure 11 (a)) the conoscopic figure observed is a set of conjugate hyperbolae, centred on a common locus<sup>49</sup>. Light that has travelled to the centre of the locus (if it is bright) will have passed along a path where the relative phase difference between the ordinary and extraordinary light is a maximum. For vertical director alignment (Figure 11 (b)), the conoscopic figure consists of concentric circular

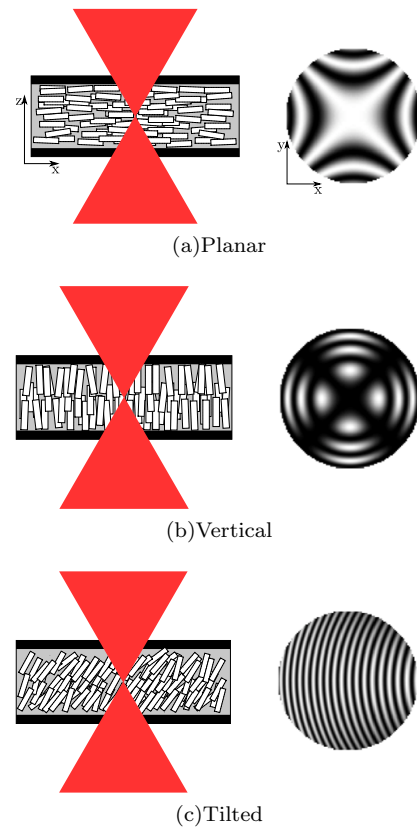


FIG. 11. Simulated conoscopic figures for the director profiles shown schematically on the left. (a) the double set of hyperbolae signalling planar alignment. (b) The maltese cross from vertical alignment of the director. (c) A series of dark fringes from a uniformly tilted sample.

fringes and a central extinction cross. Here, the centre of the cross corresponds to minimum relative phase difference<sup>49</sup>. For a director profile that is uniformly tilted (Figure 11 (c)), the conoscopic figure consists of a series of dark fringes resulting from the birefringence encountered by light passing through the cell<sup>56</sup>. This conoscopic figure is simulated for a large ( $\approx 45^\circ$ ) uniform tilt angle. For smaller tilt angles, a displacement of the locus from the centre of the field of view is observed, which, as will be seen later, can be used to estimate the tilt angle within the sample.

A modelling script was also developed by Stephen Cornford<sup>42</sup> in order to simulate the conoscopic figures observed for birefringent media. As used widely in his thesis, the Berreman<sup>57</sup> (or Jones) matrix methods were adapted to compute the conoscopic figures, as has been reported previously in the literature<sup>58,59</sup>.

Briefly, a cartesian coordinate system is defined for the computation of the conoscopic figure. Each point within that coordinate system ( $x, y$ ) can be defined by a pair of angles  $\alpha$  and  $\psi$  such that<sup>42</sup>,

$$\tan \psi = y/x \quad (38)$$

$$\sin \alpha = (x^2 + y^2)^{\frac{1}{2}} \quad (39)$$

A ray of light that passes through the focus of the cone of light at an angle of incidence  $\alpha$ , strikes the cartesian coordinate system plane with a plane of incidence at angle  $\psi$  to the figure's  $x$  axis and at an angle  $\psi'$  to the transmission angle of the polariser.

For each ray in the cone of incident light, the coefficients  $E_{ss}, E_{sp}, E_{ps}, E_{pp}$  are calculated, where  $E_{sp}$  is the complex,  $s$ -polarised component of the electric field transmitted through the sample if the incoming ray were wholly  $p$ -polarised. From these, the intensity at any point on the cartesian coordinate system can be obtained<sup>42</sup> from,

$$I(\alpha, \psi) = |(E_{pp} - E_{ps}) \sin(\psi') \cos(\psi') - E_{ps} \cos^2 \psi' + E_{sp} \sin(\psi')|^2 \quad (40)$$

In order to compute the interference figure, a set of points in the cartesian coordinate plain ( $x, y$ ) needs to be selected such that  $\sin \alpha \leq \sin \text{NA}$ , where NA is the numerical aperture of the cone of light<sup>42</sup>.

Figure ?? shows a table of simulated conoscopic figures from the computational method described above. These figures are simulated for a typical nematic liquid crystal with refractive indices of  $n_e = 1.7$  and  $n_o = 1.5$  in a cell approximately  $100 \mu\text{m}$  thick. The sequence of figures correspond to the liquid crystal uniform tilt angle  $\theta$  varying along a row, whilst the azimuthal angle  $\phi$  varies along a column.

Here as expected, for planar alignment ( $\theta = 90^\circ$ ), the conjugate set of hyperbolae centred on a common locus is computed. This set of hyperbolae is rotated as a function of the azimuthal alignment,  $\phi$  relative to the figure's  $x$  axis. For pure vertical alignment ( $\theta = 0^\circ$ ), the concentric circular fringes and maltese cross are computed. As stated earlier, for small uniform tilt angles away from either planar or vertical alignment ( $\theta = 85^\circ, 5^\circ$ ), the locus of the simulated conoscopic figure appears slightly displaced from the centre of the field of view along a line parallel to the plane containing the director azimuthal alignment angle  $\phi$ .

## O. Experimental

Figure 12 is a schematic diagram of the experimental set up that constitutes the conoscope used for analysis in this thesis. Here it is seen that firstly, light from a Helium-Neon laser (633 nm) is incident onto a rotating diffuser, acting as a scattering near point source over the small area illuminated by the beam spot. As the diffuser is rotated, the array of point sources varies, and when

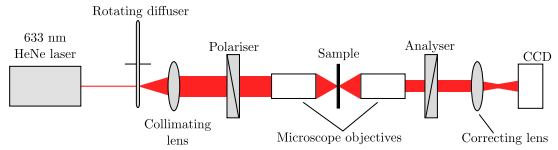


FIG. 12. A schematic diagram of the conoscope used in this research. Based on a designs from the literature<sup>59,60</sup> and built by Cornford in reference<sup>42</sup>. Here, a collimated beam passes through the polariser, main assembly and sample, before passing through the analyser and focussed on to the CCD to capture a figure.

averaged over a single rotation of the diffuser, creates a uniform cone of light, removing any speckle pattern from the laser and final conoscopic figures. The beam is then collimated before passing through the first polariser and into the first microscope objective of the main assembly.

The main assembly consists of the sample and two Mitutoyo Plan-Apo 50 $\times$  long working distance microscope objectives. The first objective takes a parallel beam of light about 3 mm in diameter, expands it, and focusses it on to the sample. The resulting convergent beam has a numerical aperture of 0.55, and a working distance of 13 mm. Having passed through the sample, the second objective collimates the beam before it passes through the second polariser, also known as the analyser.

Finally, the beam passes through a correcting lens to correct for the change in focus of the convergent beam that is generated by passing through the two thick glass plates of the sample. When the outer part of the beam exiting the second objective is parallel, the inner part is convergent (clearly visible as the beam is brighter in the centre than at the edges). On going through the correcting lens, the beam is uniform in a single plane, and that is the position where the CCD is placed<sup>42</sup>, creating a conoscopic figure which is captured from computer software for the camera used.

The following sub-sections will look at sample data images captured from the conoscope shown schematically in Figure 12. It will show (primarily for planar aligned samples) how the conoscopic figures respond to variations in certain parameters of the experimental setup, such as rotating the samples in the main assembly and rotating the polariser and analyser whilst viewing the conoscopic figure. These figures are compared to the computed figures from the optical simulation in order to confirm that the model is behaving accurately in predicting the correct conoscopic figure. Whilst the main focus of the work in this chapter, and in this thesis as a whole, is concerned with planar and near-planar aligned samples, some vertically aligned samples are included here in order to show the characteristic conoscopic figures that can be obtained.

### P. Planar alignment - rotating the cell

All planar conoscopic images included in the following sections are taken from the same liquid crystal cell which is filled with 5CB sandwiched between two glass plates spaced with un-stretched Parafilm (thickness of approximately 100  $\mu\text{m}$ ). The surface alignment layer is a rubbed polyimide. For all simulation, refractive indices for 5CB at a wavelength of 633 nm and 25 °C are used as  $n_o = 1.531$  and  $n_e = 1.706$  taken from reference<sup>30</sup>.

Firstly, Figure 13 shows how the planar conoscopic figure responds when the cell is physically rotated when in the conoscope. Here the polariser and analyser remain crossed at 0° and 90° to the image's  $x$  axis whilst the cell is rotated in increments of approximately 5°. The rubbing direction is initially at 45° to the figure's  $x$  axis (Figure 13 (a)). As the cell is rotated, the conjugate hyperbolae that make the conoscopic figure, clearly rotate until the rubbing direction becomes parallel to the polariser direction. In this position, the incident light sees only one refractive index of the liquid crystal, resulting in no average polarisation conversion of the incident light. As such, all rays arriving at the analyser are stopped and the field of view becomes completely dark (Figure 13 (i)). The same effect is also seen when the rubbing direction is exactly perpendicular to the polariser. If the cell were to be rotated through 360°, this field of view will go dark four times in total, that is, whenever the director is parallel to either the polariser or analyser.

Figure 14 now shows the simulated conoscopic figures for the same experimental setup from which the conoscopic figures in Figure 13 were obtained. This has been achieved by simulating the director profile to be aligned at varying azimuthal angles, whilst maintaining the polariser and analyser at 0° and 90° degrees respectively. It is clear that the uniaxial optics simulation provides very good agreement with the data obtained from the actual conoscope. As the azimuthal alignment of the director is changed, the field of view goes from showing the conjugate set of hyperbolae to going completely dark when the director and polariser or analyser are parallel with one another (Figure 14 (i)).

### Q. Planar alignment - rotating the polarisers

A second experiment was also carried out, in which the cell was maintained in the same orientation (director at 45° to the image's  $x$  axis) but now, the polariser and analyser were rotated in 10° increments whilst always remaining at 90° to one another (crossed). The conoscopic figures obtained can be seen in Figure 15, images (a) to (j). As expected, the conjugate hyperbolae which make up the conoscopic figure remain undistorted, whilst the field of view gets darker before becoming completely black when either the polariser or analyser are aligned parallel to the rubbing direction (f). As the polariser and analyser are rotated past being parallel to the rub-

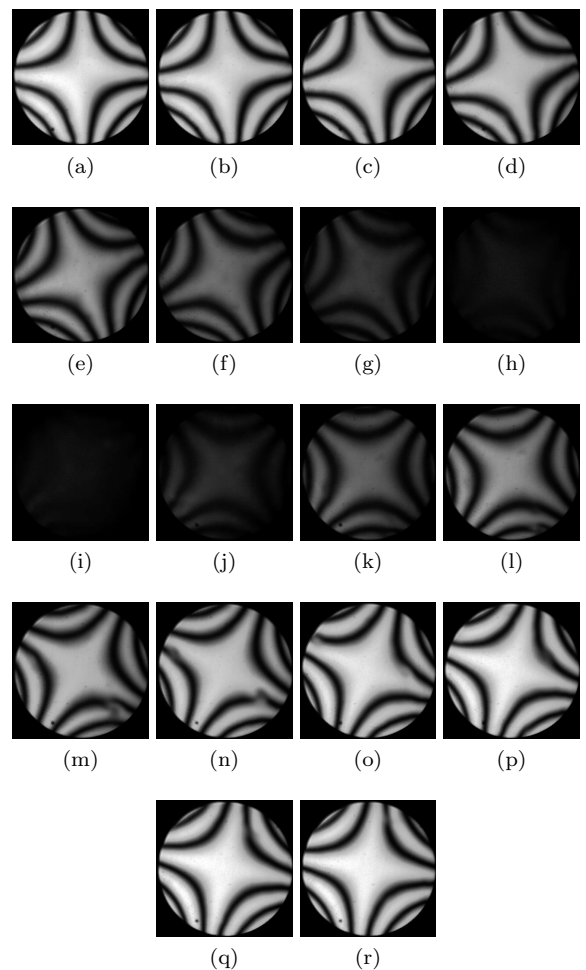


FIG. 13. Data conoscopic figures for a planar aligned cell. The polariser and analyser remain crossed at 0° and 90° to the figure's  $x$  axis whilst the cell is rotated in increments of approximately 5° through images (a) to (r). When the cell is rotated so that the rubbing direction becomes parallel to either the polariser or analyser (image (i)), the field of view is shown to be completely dark. This is due to the incident light experiencing only one of the refractive indices of the liquid crystal, resulting in no polarisation conversion and all light being blocked by the analyser.

bing direction, the field of view becomes brighter again, returning to the initial conoscopic figure.

Figure 16 again shows the simulated conoscopic figures for the same experimental set up, in which the alignment angle in the cell remains constant, and the polariser and analyser are rotated in 10° increments whilst always remaining crossed to one another. Here again, it is clear that the uniaxial optics simulation provides very good agreement with the data obtained from the conoscope. As the polariser and analyser are rotated, the field of view goes from showing the conjugate set of hyperbolae to appearing completely dark when the director and polariser or analyser are parallel with each other (Figure 16

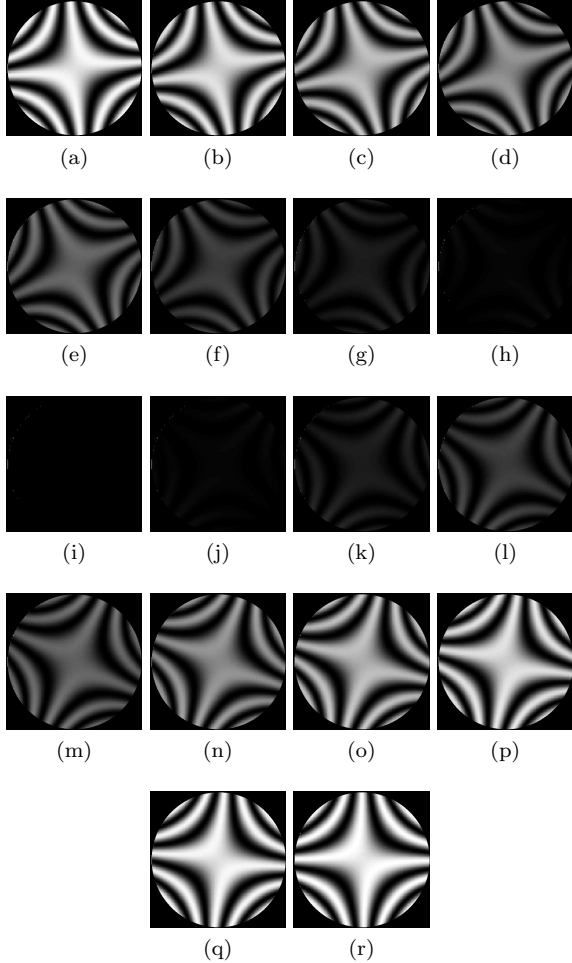


FIG. 14. Simulated conoscopic figures as the director azimuthal alignment is rotated in increments of  $5^\circ$  from (a) to (r). These figures can be directly compared to the data conoscopic figures shown in Figure 13 where a good agreement is seen.

(f)).

### R. Planar alignment - thickness variation

Figure 17 demonstrates how the planar alignment conoscopic figure varies as a function of the cell thickness. The conoscopic figures in Figure 17 were achieved by tracking across the cell in the  $x - y$  plane with each image (a) to (g) taken at a different point. Here it is shown that the conjugate set of hyperbolae can move into and out of the centre of the conoscopic figure. As the cell thickness increases, there will be more fringes visible within the field of view. Conversely, as the cell thickness decreases, there will be fewer fringes in the field of view. This effect of cell thickness on fringe number is also true in the case of a vertically aligned sample (shown later in Figure 18), where extra sets of concentric circular fringes

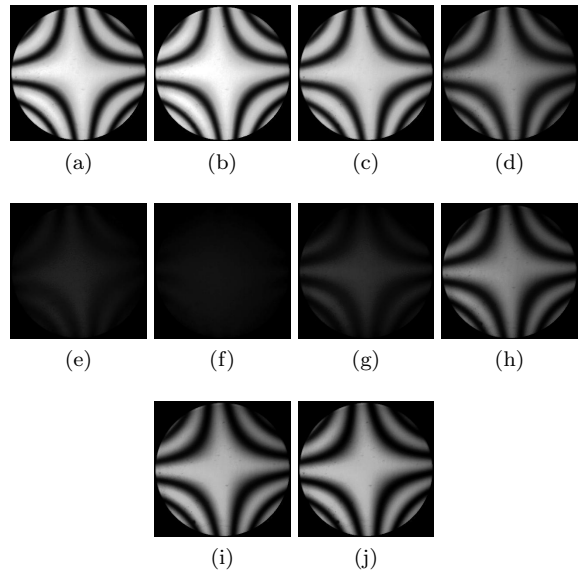


FIG. 15. Planar cell with the rubbing direction at  $45^\circ$  to the  $x$  axis. The polariser and analyser remain crossed to one another whilst they are rotated in approximately  $10^\circ$  increments from (a) to (j)

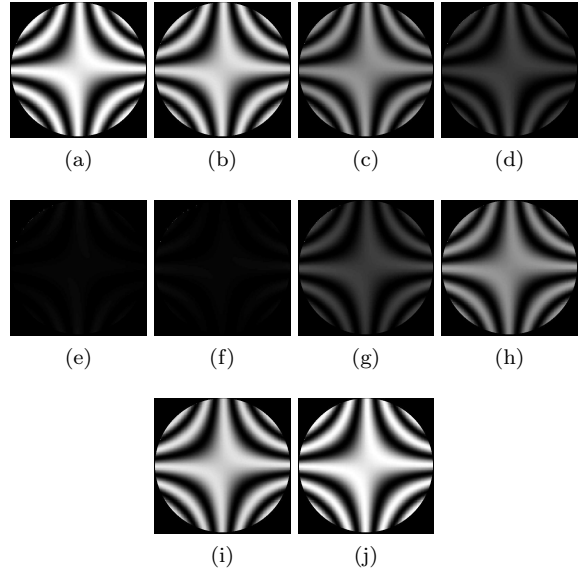


FIG. 16. Simulated conoscopic figures whereby the polariser and analyser remain crossed to one another and are rotated in increments of  $10^\circ$  from (a) to (j). These figures can be directly compared to the data conoscopic figures shown in Figure 15 whereby a good agreement is seen.

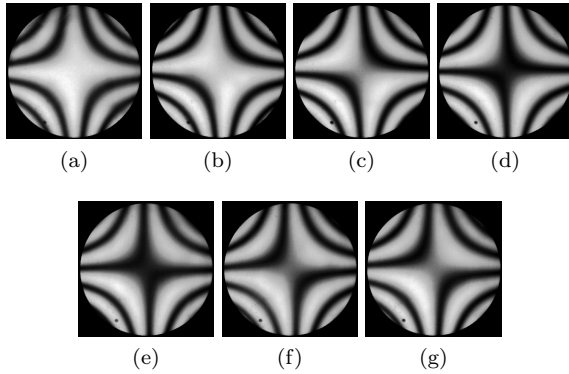


FIG. 17. Conoscopic interference figure for a planar cell rubbed at  $45^\circ$  to the figure's  $x$  axis. Polariser and analyser are crossed and at  $0^\circ$  and  $90^\circ$  to the figure's  $x$  axis. Figures (a) through (g) show how the figure changes when moving the cell approximately 5 mm in the  $x$ -direction due to a depth gradient across the cell.

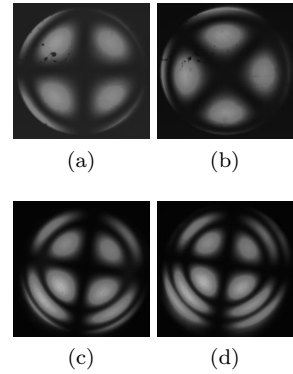


FIG. 18. Data conoscopic figure captures of a cell aligned vertically through a surface treatment of lecithin dissolved in ether. Figures (a) and (b) show figures where the crossed polarisers are at  $0^\circ$  and  $45^\circ$  to the  $x$  axis respectively. Figures (c) and (d) depict a vertically aligned cell whereby (d) is captured in a slightly thicker part of the cell, with more fringes visible around the maltese cross.

can be seen as the cell thickness increases. In Figure 17, the director is aligned at  $45^\circ$  to the figure's  $x$  axis, and most importantly, there is very little change in this angle of orientation as the cell is moved around. This demonstrates that the rubbed polymer alignment layer has produced spatially coherent director alignment over a relatively large area (millimetres) of the cell.

### S. Vertical alignment

Figure 18 shows captured conoscopic figures for a cell that has been aligned vertically through a surface treatment of lecithin dissolved in ether<sup>61</sup>. Here it is shown that the conoscopic figure consists of (as described earlier) concentric circular fringes and a central extinction cross that is often referred to as the 'classic' maltese cross. Figure 18 (a) and (b) show captured conoscopic figures for the same vertically aligned cell whereby the polariser and analyser are crossed  $0^\circ$  and  $90^\circ$  to the  $x$  axis, and at  $45^\circ$  and  $135^\circ$  to the  $x$  axis respectively. This difference in polariser/analyser alignment is shown by the rotation of the extinction cross through  $45^\circ$ . Figures 18 (c) and (d) show two conoscopic figure captures from a different cell, in which a thickness gradient exists. Much like in the case of the planar conoscopic figure example (Figure 17) the number of concentric circular fringes visible at the edge of the field of view increases as the cell becomes thicker. This is visible when looking at image (c) with just one set of fringes and image (d) which contains two sets of fringes<sup>62</sup>.

### T. Polarisers crossed and parallel

Finally, Figure 19 shows a comparison between planar aligned and vertically aligned captured conoscopic figures viewed when the polariser and analyser are crossed to one another (a) and (c) and also when the analyser has been rotated to become parallel to the polariser (b) and (d). These figures were again captured as a test to see whether the conoscope was working as expected. For both cases, the conoscopic figures captured when the polariser and analyser are parallel to one another appear to be the inverse of the figures where the polariser and analyser are crossed to one another. This is as expected. When the analyser is rotated to be parallel to the polariser, any light that exits the cell polarised orthogonal to the analyser will be blocked, resulting in a dark area on the conoscopic figure. When the analyser is rotated through  $90^\circ$  to be parallel to the polariser, this same light will be passed by the analyser, resulting in a light area on the conoscopic figure. This is shown by Figure 19 (b) now having a dark centre, and most strikingly the inverse vertically aligned conoscopic figure whereby a light cross is formed by four dark lobes.

### U. Tracking conoscopic figure alignment

In order to accurately determine the alignment angle of the conjugate hyperbolae present in the planar conoscopic figure, a computer minimisation routine was created to automatically iterate down to the correct angle. Typical output figures from this program can be seen in Figure 20. Before the automated routine can be run, the conoscopic figures must be lightly processed in order for them to work with the computer program. This pro-

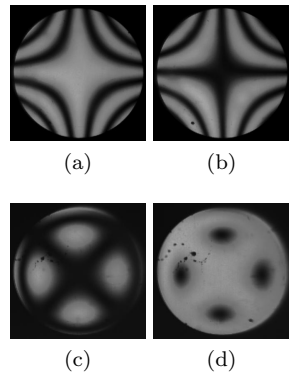


FIG. 19. A comparison between data conoscopic figures for a planar aligned cell and a vertically aligned cell viewed when the polariser and analyser are crossed to one another and also when they are parallel to one another. Images (a) and (b) show a planar aligned cell viewed conoscopically between crossed and parallel polarisers respectively. Images (c) and (d) show a vertically aligned cell viewed conoscopically between crossed and parallel polarisers respectively. In both cases, the conoscopic figures are essentially the inverse of the original.

cessing involves cropping the images to be square, and smoothing the figures to remove any artefacts that may give misleading results (simple gaussian smoothing in ImageJ is suitable for this). Examples of an original simulated planar conoscopic figure and the smoothed version can be seen in Figure 20 (a) and (b).

In order to accurately determine the angle at which the hyperbolae are aligned, the program plots an initial line running through the centre of the field of view at a pre-defined angle (normally measured from the  $x$  axis of the figure). Two further test lines are then plotted parallel and at a fixed distance to the initial line. The automated routine then plots the values of the pixel intensities along these two test lines and plots them as a function of position along the test line. Pairs of images can be seen in Figure 20 (c) to (j) in which the test lines plotted on the conoscopic figure (left column) correspond to the pixel intensities as a function of position on the line (plotted in the right column). The program then alters the angle at which the initial line is plotted (each time re-plotting two new parallel test lines) and measuring the difference between the pixel intensities for this given initial line. The automated routine varies the initial line angle to iterate down to a line which best minimises the difference in sum of the pixel intensities between the two test lines. At this point, the angle of the plotted line defines the angle at which the conjugate hyperbolae of the conoscopic figure are aligned.

For example, Figure 20 (c) shows the initial line and the two test lines plotted either side for the first iteration. It is clear by eye that the initial guess does not minimise the difference in pixel intensities of the two lines, although this is confirmed in (d) whereby the pixel inten-

sities along the test lines in image (c) are plotted. It is clearly visible that the data points and line do not overlap each other. The second iteration (images (e) and (f)) make the situation even worse, with a bigger difference between the plotted pixel intensities. Accordingly, the third iteration moves the test line in the opposite direction ((g) and (h)) and a smaller difference between the test line pixel intensities is found. After the fourth iteration, the difference between the test line pixel intensities is minimised ((i) and (j)) and the angle at which the test lines are plotted over the conoscopic figure is returned by the program. In practice, this process may take more than four iterations, but is a valuable tool in systematically and automatically ascertaining the alignment angle of the conjugate hyperbolae of the planar conoscopic figure.

As will be seen in later chapters, the fits between the plotted pixel intensities are far worse when the automated routine is carried out on actual conoscopic figures as opposed to here where the simulated noise-free figures provide easy minimisation and near perfect evaluation of the alignment angle.

This chapter will now go on to discuss the cell fabrication methods developed during this study in order to conduct the pressure driven flow experiments that will be detailed in the following chapters.

## V. Cell fabrication

In order to conduct dynamic pressure driven flow experiments, robust cells that allow flow of a liquid crystal from a syringe drive must be fabricated. During the course of this investigation, a set technique has been developed, refined and improved upon, to become what is now a standard process for the production of pressure driven flow cells within the group at Exeter.

Cells are generally constructed from a standard glass microscope slide that has been cut in half to produce two approximately 3 cm by 2 cm plates. One of the plates is drilled with holes by our workshop technicians to allow for the inlet/outlet pipes to be attached. The plates are then cleaned (see below), before having a surface alignment layer deposited, and rubbed if necessary.

## W. Microscope slide preparation

1. All cleaning of microscope slides and cover slips is carried out in clean tents, where fans perpetually circulate the air in the immediate environment. All processes are also carried out wearing latex gloves to minimise contamination with skin grease or other foreign bodies from the immediate environment.
2. Slides are removed from their sealed container and firstly cleaned rigorously with a cotton bud soaked

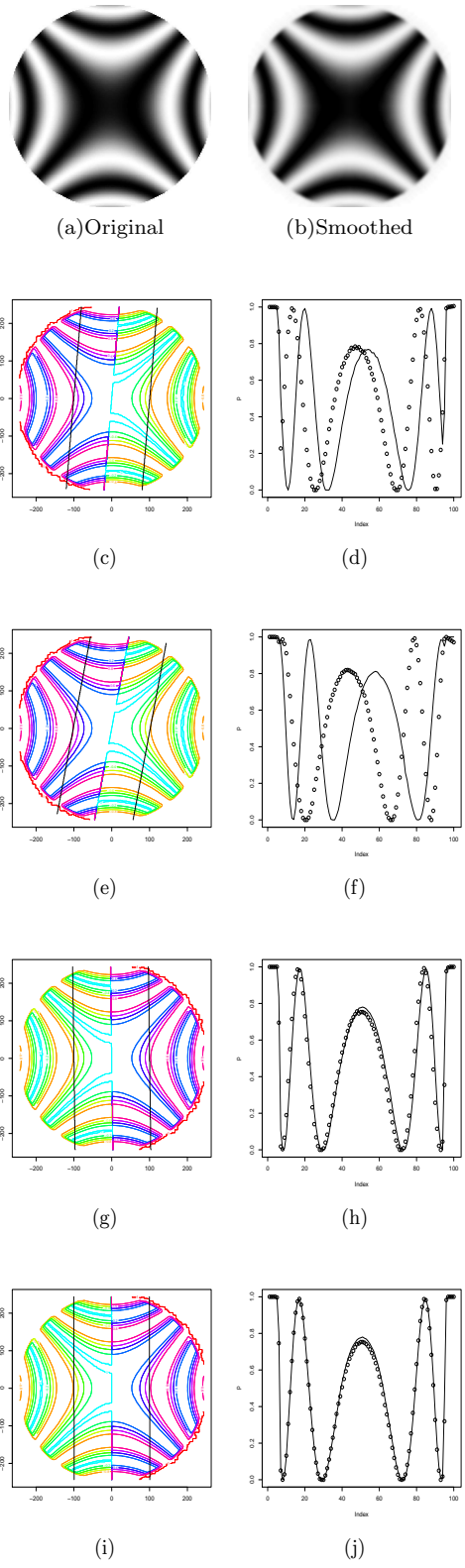


FIG. 20. (a) Original simulated conoscopic figure. (b) Original figure after smoothing in ImageJ. Images (c) to (j) show pairs of images whereby the pixel intensities plotted along the two lines either side of the central test line are plotted. After three iterations, the difference between the left and right test lines has been minimised resulting in determination of the azimuthal alignment angle of the conoscopic figure.

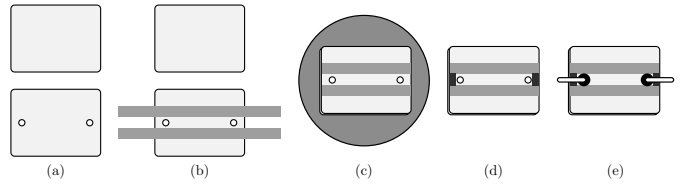


FIG. 21. (a) The glass slides are placed on a clean and flat surface ready for cell construction. (b) Stretched strips of *Parafilm* are placed either side of the inlet/outlet holes to define a flow channel. (c) The plates are sandwiched together and the excess *Parafilm* is removed. The cell is then placed on a hot plate to bond the *Parafilm* to the glass. (d) UV curing glue is introduced to seal the channel ends and cured under a UV lamp. (e) Inlet and outlet pipes are attached to the flow cell with an epoxy resin adhesive.

in acetone. Initially they are rubbed with firm pressure in one direction and then rubbed again at  $90^\circ$  to the initial cleaning direction. This technique is considered to be a mechanical cleaning process to get rid of any debris or small particles that may be on the surface of the slide. The acetone also aids in removing any grease or smudges that are present on the slides<sup>63</sup>.

3. Step 2 is then repeated with cotton buds soaked in isopropanol (IPA). This step removes any residue left by the acetone on the surface of the slide. The slides are then blasted with an inert dusting gas to remove any fibres that may have been left by the cotton buds.
4. Finally, and most importantly, the slides are drag cleaned with lens tissue soaked in IPA. The lens tissue is placed over the slide and pulled slowly (at approximately the same rate that the IPA evaporates) across the slide with tweezers. This process removes any smears or debris left by the previous stages. This step can be repeated several times until the slide is free of any defects when examined by eye.

## X. Cell construction

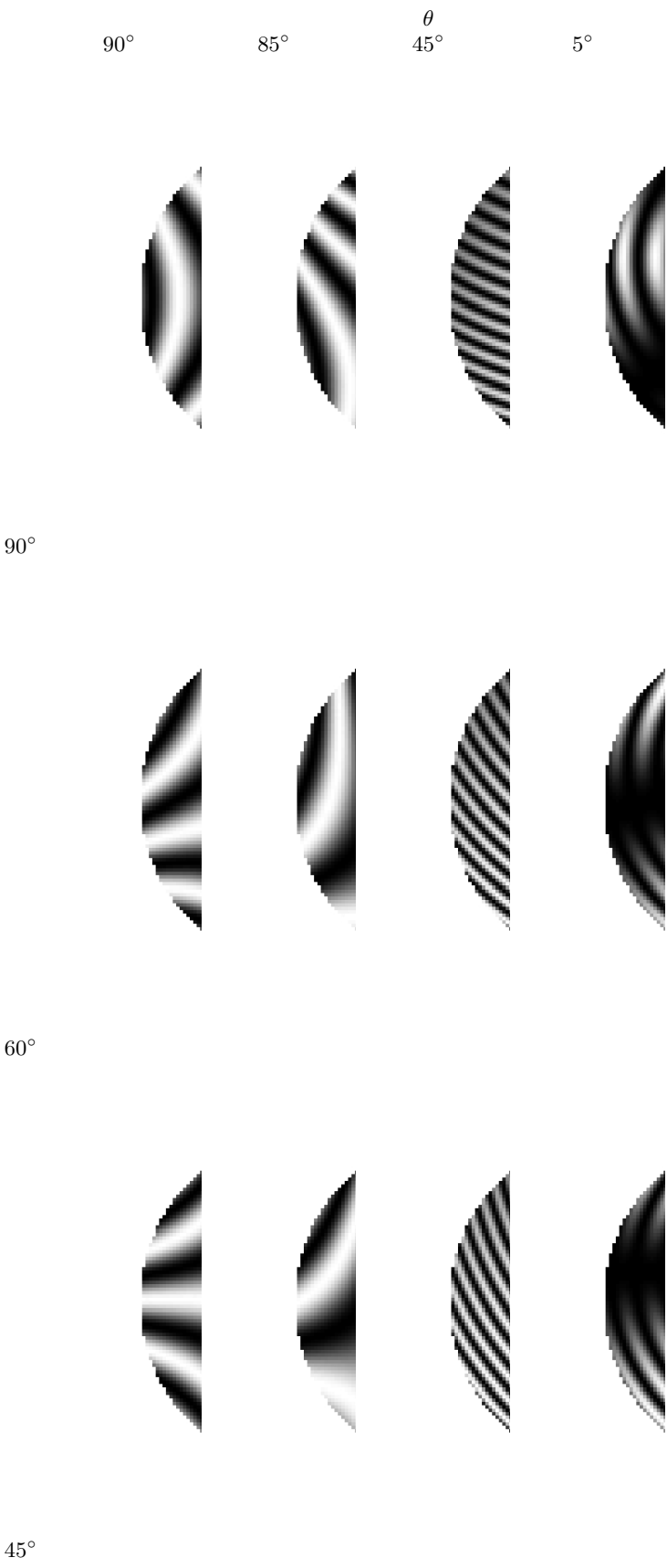
At this stage, aligning layers can be deposited onto the glass slides. Conventionally this is done by spin coating a layer of polyimide in order to align the director, whereby the particular composition of the polymer promotes a particular alignment. Once the glass slides have been prepared with an alignment layer, they are ready to be brought together to form a flow cell. Figure 21 shows a schematic diagram of this process.

1. Firstly, the slides are placed on a flat clean surface and arranged so that the top plate can be placed on top of the bottom plate to create the initial alignment conditions required.

#### IV THEORY / METHODS

2. Two thin strips of *Parafilm* are cut and stretched by hand to form the walls of the flow channel. Prior to stretching, the *Parafilm* is approximately 120  $\mu\text{m}$  thick, once stretched, this is reduced to approximately 45  $\mu\text{m}$ . These strips are placed on either side of the inlet and outlet holes, defining a flow channel that is approximately 3 mm in width. The two slides are then sandwiched together under a moderate pressure. The surplus pieces of *Parafilm* are removed with a scalpel.
3. The cell is placed on a hot plate at approximately 60 °C, or until the *Parafilm* becomes tacky and bonds the two glass plates together. During this time, a cotton bud can be used to apply pressure to the *Parafilm* walls, flattening and aiding the bonding process.
4. A UV curing glue (Norland optical adhesive) is applied by a cocktail stick to the open ends of the flow channel. This then capillary fills into the cell. Great care must be taken to apply only a very small amount of glue to the cell, as it can fill too far up the flow channel and block either the inlet or outlet hole. The cell is then placed under a UV lamp for approximately 15 minutes, or until the glue has cured.
5. Finally, steel inlet (and outlet if necessary) tubes are glued to the cell with an epoxy resin. To aid the bonding process, the bottom surface of the brass collar surrounding the inlet/outlet tube can be roughened with a file or scalpel. The advent of brass collars to secure the pipe to the cell at the inlet and outlet holes has been a key development in fabricating robust and well sealed flow cells, as shown in Figure ???. In some cases, the area of the glass cell around the inlet hole can be masked off and roughened with an air sand blaster. This process can aid the strength of the bonding between the collar and the glass.

A diagram showing a typical flow cell in relation to the syringe drive and conoscope for the experiments described in the following chapters is given in Figure ???. The flow cell is connected to a syringe pump and is placed at the convergent point of the cone of light in the conoscope.



#### IV THEORY / METHODS

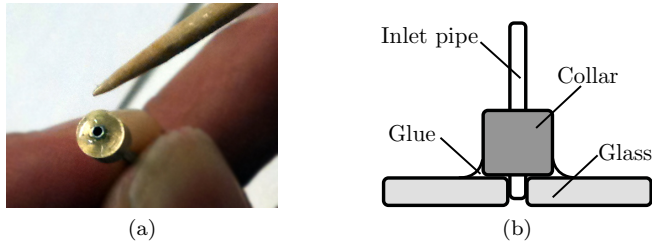


FIG. 22. (a) Shows a photograph of epoxy resin being applied to a collar with a cocktail stick. (b) A schematic diagram of the collar on the pipe as it is inserted into a slide. The collar and glue form a robust contact around the joint ensuring there is no leakage.

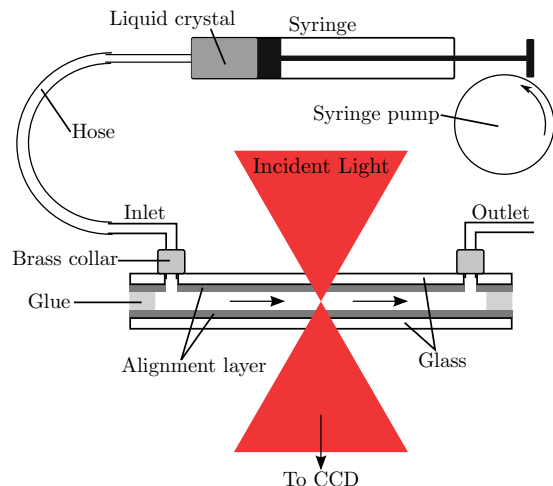


FIG. 23. A schematic representation of a flow cell in relation to the syringe drive and convergent part of the conoscopic beam.

- \* c.holmes4@gmail.com
- <sup>1</sup> F. Reinitzer, Monatshefte fur Chemie (Wien) **9**, 421 (1888).
  - <sup>2</sup> T. J. Sluckin, D. A. Dunmur, and H. Stegemeyer, *Crystals that flow: classic papers from the history of liquid crystals* (Taylor and Francis, 2004).
  - <sup>3</sup> D. W. Bruce, J. W. Goodby, J. R. Sambles, and H. J. Coles, *Philosophical transactions. Series A, Mathematical, physical, and engineering sciences* **364**, 2567 (2006).
  - <sup>4</sup> P. J. Collings and M. Hird, *Introduction to liquid crystals* (Taylor and Francis, 1997).
  - <sup>5</sup> J. Burroughes, D. Bradley, A. Brown, R. Marks, K. Mackay, R. Friend, P. Burns, and A. Holmes, *Nature* **347**, 539 (1990).
  - <sup>6</sup> J.-B. Fleury, D. Pires, and Y. Galerne, *Physical Review Letters* **103**, 267801 (2009).
  - <sup>7</sup> C. T. Imrie, *Liquid Crystals* **37**, 497 (2010).
  - <sup>8</sup> Z. Nguyen, M. Atkinson, C. Park, J. MacLennan, M. Glaser, and N. Clark, *Physical Review Letters* **105**, 1 (2010).
  - <sup>9</sup> F. Vollrath and D. P. Knight, *Nature* **410**, 541 (2001).
  - <sup>10</sup> J. Lydon, *Liquid Crystals Today* **13**, 1 (2004).
  - <sup>11</sup> G. Gupta and A. Rey, *Physical Review Letters* **95**, 3 (2005).
  - <sup>12</sup> F. Müller, U. Kornek, and R. Stannarius, *Physical Review E* **75**, 1 (2007).
  - <sup>13</sup> J. C. Bird, R. de Ruiter, L. Courbin, and H. a. Stone, *Nature* **465**, 759 (2010).
  - <sup>14</sup> a. Fernández-Nieves, V. Vitelli, a. Utada, D. Link, M. Márquez, D. Nelson, and D. Weitz, *Physical Review Letters* **99**, 1 (2007).
  - <sup>15</sup> F. Bawden, N. Pirie, J. Bernal, and I. Fankuchen, *Nature* , 1051 (1936).
  - <sup>16</sup> M. Lettinga and E. Grelet, *Physical Review Letters* **99**, 197802 (2007).
  - <sup>17</sup> A. Tkachenko, *Physical review letters* **77**, 4218 (1996).
  - <sup>18</sup> W. Helfrich, *Physical Review Letters* **23**, 372 (1969).
  - <sup>19</sup> E. Yablonovitch, *Physical review letters* **58**, 2059 (1987).
  - <sup>20</sup> M. Humar and I. Mušević, *Optics Express* **18**, 26995 (2010).
  - <sup>21</sup> J. Schäfer, J. P. Mondia, R. Sharma, Z. H. Lu, a. S. Susha, a. L. Rogach, and L. J. Wang, *Nano letters* **8**, 1709 (2008).
  - <sup>22</sup> J. W. Doane, N. a. Vaz, B.-G. Wu, and S. Zumer, *Applied Physics Letters* **48**, 269 (1986).
  - <sup>23</sup> I. I. Smalyukh, a. N. Kuzmin, a. V. Kachynski, P. N. Prasad, and O. D. Lavrentovich, *Applied Physics Letters* **86**, 021913 (2005).
  - <sup>24</sup> M. Yada, J. Yamamoto, and H. Yokoyama, *Physical Review Letters* **92**, 1 (2004).
  - <sup>25</sup> G. Vertogen and W. H. de Jeu, *Thermotropic Liquid Crystals, Fundamentals* (Springer-Verlag, 1988).
  - <sup>26</sup> J. Lydon, *Liquid Crystals Today* **15**, 1 (2006).
  - <sup>27</sup> T. S. Taphouse, *Time Resolved Optical Characterisation of Hybrid Aligned Nematic Liquid Crystal Cells*, Ph.D. thesis (2007).
  - <sup>28</sup> G. Friedel, *Annales de Physique* **18**, 273 (1922).
  - <sup>29</sup> There are many smectic phases, running from  $S_A, S_B, \dots, S_I$ , differing in molecular orientation and layer spacing.
  - <sup>30</sup> J. Li, C.-h. Wen, S. Gauza, R. Lu, and S.-t. Wu, **1**, 51 (2005).
  - <sup>31</sup> I. Stewart, *The static and dynamic continuum theory of liquid crystals: a mathematical introduction* (Taylor & Francis, 2004).
  - <sup>32</sup> M. Miesowicz, *Nature* **158** (1946).
  - <sup>33</sup> For the liquid crystal PPA at 122° C (in the nematic phase).
  - <sup>34</sup> The notation adopted here is the notation used by Miesowicz, but some texts adopt the Helfrich notation<sup>64</sup> which interchanges the above definitions of  $\eta_1$  and  $\eta_2$ .
  - <sup>35</sup> J. a. Janik, *Liquid Crystals Today* **2**, 6 (1992).
  - <sup>36</sup> T. Carlsson and F. M. Leslie, *Liquid Crystals* **26**, 1267 (1999).
  - <sup>37</sup> F. M. Leslie, *Continuum Mech. Thermodyn.* **4**, 167 (1992).
  - <sup>38</sup> For a rigorous analysis of equation 6 and a full derivation of the dissipation function (equation 7), the reader is directed to the *Static and Dynamic Continuum Theory of Liquid Crystals* by Iain W. Stewart<sup>31</sup>, which gives a comprehensive mathematical introduction to the dynamic theory of nematic liquid crystals.
  - <sup>39</sup> V. Belyaev, *Physics-Uspekhi* **44**, 255 (2001).
  - <sup>40</sup> O. Parodi, *Journal de Physique* **31**, 581 (1970).
  - <sup>41</sup> P. K. Currie, *Molecular Crystals and Liquid Crystals* **28**, 335 (1974).
  - <sup>42</sup> S. Cornford, *eric.exeter.ac.uk*, Ph.D. thesis, University of Exeter (2008).
  - <sup>43</sup> J. E. Birkett, *Chiral HAN cells: a novel liquid crystal arrangement*, Ph.D. thesis, University of Exeter (2008).
  - <sup>44</sup> S. Jewell, *Cell*, Ph.D. thesis, Exeter (2002).
  - <sup>45</sup> The model described here takes into account the possibility of an applied electric field through ITO coated substrates, the flexoelectric effect or space charges.
  - <sup>46</sup> R. P. Feynmann, R. B. Leighton, and M. Sands, *The Feynmann Lectures on Physics, Volume II* (Addison-Wesley, 1964) p. Chapter 41.
  - <sup>47</sup> Some relevant material is included in references<sup>65</sup> and<sup>66</sup>.
  - <sup>48</sup> “<http://en.wikipedia.org/wiki/Conoscopy>,”.
  - <sup>49</sup> B. Henning and Others, *Appl. Opt* **40**, 2089 (2001).
  - <sup>50</sup> S. L. Cornford, T. S. Taphouse, and J. R. Sambles, *New Journal of Physics* **11**, 013045 (2009).
  - <sup>51</sup> F. Yang, S. A. Jewell, L. Ruan, and J. R. Sambles, *Journal of the Optical Society of America B* **24**, 527 (2007).
  - <sup>52</sup> S. A. Jewell, T. S. Taphouse, and J. R. Sambles, *Applied Physics Letters* **87**, 021106 (2005).
  - <sup>53</sup> S. A. Jewell and J. R. Sambles, *Physical Review E* **73**, 011706 (2006).
  - <sup>54</sup> S. A. Jewell and J. R. Sambles, *Molecular Crystals and Liquid Crystals* **477**, 551 (2007).
  - <sup>55</sup> White light can also be used.
  - <sup>56</sup> The conoscopic images shown in Figure 11 are calculated from the uniaxial modelling script described later.
  - <sup>57</sup> D. W. Berreman, *J. Opt. Soc. Am* **62**, 502 (1972).
  - <sup>58</sup> T. Ogasawara, T. Akizuki, Y. Takanishi, K. Ishikawa, and H. Takezoe, *Mol. Cryst. Liquid Cryst.* (2001).
  - <sup>59</sup> L. Parry-Jones, E. Kriegis, and S. Elston, *Japanese Journal of Applied Physics* **41**, L1485 (2002).
  - <sup>60</sup> T. Fujikawa, K. Hiraoka, T. Isozaki, K. Kajikawa, H. Takezoe, and A. Fukuda, *Japanese Journal of Applied Physics* **32**, 985 (1993).
  - <sup>61</sup> In order to achieve a good alignment layer, a small amount of lecithin is dissolved in the ether until the solution becomes pale yellow in colour. The face is then coated by dragging a lens tissue soaked in the solution across the

## V ALEX

glass surface.

<sup>62</sup> The slight displacement of the locus from the centre of the field of view in Figure 18 (c) and (d) when compared with (a) and (b) suggests that the director may be slightly tilted away from vertical alignment.

<sup>63</sup> One must take care not to use the same end of the cotton bud twice as this can result in contamination of the solvent reservoir.

<sup>64</sup> W. Helfrich, J. Chem. Phys. **51**, 4092 (1969).

<sup>65</sup> Z. Cui, M. Gregory Forest, Q. Wang, and H. Zhou, SIAM Journal on Applied Mathematics **66**, 1227 (2006).

<sup>66</sup> E. P. Choate, Z. Cui, and M. Gregory Forest, Rheologica Acta **47**, 223 (2008).

## V. ALEX



Alex - thank you for your help, advice and friendship during my time at Exeter. You are sorely missed.